Electronic Supplementary Material (ESI) for ChemComm.
This journal is © The Royal Society of Chemistry 2023

Molybdenum(IV) β-Diketonate Complexes as Highly Active Catalysts for Allylic Substitution Reactions

Fabio Masero[a], Prof. Dr. Victor Mougel*[a]

[a] Laboratory of Inorganic Chemistry (LAC), Department of Chemistry and Applied Biosciences (D-CHAB), ETH Zurich, Vladimir-Prelog Weg 2, 8093 Zurich, Switzerland. Email: mougel@inorg.chem.ethz.ch

Supporting Information

1. Experimental

General Information: If not stated otherwise, all manipulations were conducted under air- and water free conditions under argon, either using standard glovebox (Vigor) or Schlenk-line techniques. All glassware was stored overnight at 120 °C and cooled under dynamic vacuum. Caps, valves, syringes *etc.* containing plastic and/or Teflon were dried overnight in a vacuum oven (T = 60 °C, p = 10^{-3} mbar) prior to use. Dry solvents were obtained from a solvent purification system (Vigor), degassed by three consecutive freeze pump thaw cycles, and stored in a glove box, in J. Young-valve equipped flasks over activated molecular sieves (for additional purification details, see Table S1). Deuterated solvents were degassed by three consecutive freeze pump thaw cycles and purified according to Table S2. Commercially available chemicals were used as received or purified according to Table S3.
NMR spectra were obtained on a 300 MHz Bruker Avance III spectrometer. VT NMR spectra were recorded on a Bruker AVANCE DRX 500 MHz NMR spectrometer. ^{1}H and ^{13}C NMR spectra were referenced to residual protonated solvent signals. UV-Vis spectra were collected inside an argon filled glove box with an Agilent Cary 60 instrument, which was connected by an optical fiber to a dip probe (path length d = 2 mm). Magnetic susceptibility measurements in the solid state were carried out on a Gouy Balance (Johnson Matthey). Elemental analyses were performed by the Mikrolabor ETH Zurich on a LECO TruSpec Micro spectrometer.

Table S1: List of used solvents, supplier and purification.

Solvent	Supplier	Purification
Acetonitrile (MeCN)	Aldrich	From SPS, stored over 3 Å MS.
Benzene (C_6H_6)	Aldrich	Distilled from K/benzophenone, stored over 4 Å MS.
Diethylether (Et_2O)	Aldrich	From SPS, distilled from K/benzophenone, stored over 4 Å MS.
Dichloromethane (CH_2Cl_2)	Aldrich	From SPS, stored over 4 Å MS.
1,2-Dimethoxyethane (DME)	Aldrich	Distilled from K/benzophenone, stored over 4 Å MS.
^{n}Pentane	Aldrich	From SPS, stored over 4 Å MS.
Pyridine (Py)	Aldrich	Distilled from K/benzophenone, stored over 4 Å MS.
Tetryhydrofuran (THF)	Aldrich	From SPS, distilled from K/benzophenone, stored over 4 Å MS.
Toluene (PhMe)	Chemie Brunschwig	From SPS, stored over 4 Å MS.

Table S2: List of used deuterated solvents, supplier and purification.

Solvent	Supplier	Purification
MeCN-d_3	Aldrich	Stored over 3 Å MS (2 x 48 h)
Benzene-d_6	Aldrich	Distilled from K/benzophenone, stored over 4 Å MS.
CD_2Cl_2	Chemie Brunschwig	Distilled from CaH_2, stored over 4 Å MS.
$CDCl_3$	Aldrich	Distilled from CaH_2, stored over 4 Å MS.

Table S3: List of commercially available compounds.

Reagent	Supplier	Purification
Acetylacetone (acacH) ≥ 99.5%	Aldrich	Degassed by freeze pump thaw (3x).
Dipivaloylmethane (dpmH)	Fluorochem	Degassed by freeze pump thaw (3x).
Dibenzoylmethane (dbmH) 98%	Aldrich	Recrystallized from MeOH and dried under vacuum (10^{-3} mbar).
Hexafluoroacetylacetone (hfacac) 98%	Aldrich	Degassed by freeze pump thaw (3x).
$MoCl_5$ anhydrous 99.6%	Strem-Chemicals	Dried under vacuum (10^{-3} mbar) for 24 h.
Silver trifluoromethane-sulfonate (AgOTf) 99%	Fluorochem	Dried under vacuum (10^{-3} mbar) for 24 h.
Silver hexafluoroantimonate ($AgSbF_6$) 99%	AlfaAesar	Dried under high vacuum (10^{-6} mbar) for 24 h.
Cinnamyl alcohol 98%	Aldrich	Dried under vacuum (10^{-3} mbar) for 24 h.
Phenol (PhOH) 99%	Acros	Sublimed under vacuum (10^{-3} mbar).
p-Cresol 99+%	Acros	Distilled from P_2O_5, degassed by freeze pump thaw (3x), stored over 4 Å MS.
Trimethylsilyl azide > 95%	Tokyo Chemical Industry	Fractional distillation, degassed by freeze pump thaw (3x).
2-Methyl-3-buten-2-ol ≥ 97%	Fluka-Chemie AG	Degassed by freeze pump thaw (3x), stored over 4 Å MS,
CH_2Br_2 > 99%	Tokyo Chemical Industry	Used as received.

2. Synthesis of Coordination Complexes

2.1 General Procedure for the Preparation of $[Mo^{IV}(^{R}diket)_2Cl_2]$ ($^{R}diket$ = β-diketonate)

This procedure was adapted from van den Bergen *et al..*[1] $MoCl_5$ (1 equiv.) and acetonitrile (MeCN, 0.15 M) were placed in a Schlenk flask, equipped with a reflux condenser and refluxed at 85 °C for 3 h. The mixture was allowed to cool, the β-diketone ligand (3 equiv.) was added under stirring and then further refluxed at 85 °C for 12 h. After cooling to room temperature, the resulting precipitate was collected by filtration, washed with cold MeCN (2x), and dried *in vacuo*, affording the desired Mo(IV)-complexes as solids. For further purification steps, see below.

2.1.1 Synthesis of $[Mo(^{Me}diket)_2Cl_2]$

The title compound was prepared according to the general procedure described above from $MoCl_5$ (1.70 g, 6.22 mmol, 1.0 equiv.) and ^{Me}diketH (1.34 mL, 13.1 mmol, 2.1 equiv.), resulting in the formation of a dark red solid. The crude product was further purified by recrystallization from hot MeCN, affording the desired complex as a dark microcrystalline material. Yield: 1.12 g (3.07 mmol, 49%). Anal. Calcd for $C_{10}H_{14}O_4Cl_2Mo$: C, 32.90; H, 3.87. Found: C, 32.86; H, 3.86; N, <0.2%. μ_{eff} = 2.67 μ_B (Gouy balance). Single crystals suitable for XRD analysis were grown upon storing a saturated MeCN solution at -35 °C (see Section S3 for details). Very low solubility in common organic solvents prevented us from recording solution NMR spectra of this compound.

2.1.2 Synthesis of [Mo(^{tBu}diket)$_2$Cl$_2$]

The title compound was prepared according to the general procedure described above from $MoCl_5$ (6.0 g, 22.0 mmol, 1.0 equiv.) and ^{tBu}diketH (13.8 mL, 66.0 mmol, 3 equiv.) resulting in the formation of an orange crystalline solid. The crude product was further purified by recrystallization from hot MeCN. Co-crystallized MeCN was removed by dissolving the crystalline solid in THF, taking it to dryness, followed by rinsing it with Et_2O (2x) and drying *in vacuo* (2x), affording analytically pure [Mo(^{tBu}diket)$_2$Cl$_2$] as an orange microcrystalline powder. Yield: 7.87 g (14.8 mmol, 67%). Anal. Calcd for $C_{22}H_{38}O_4Cl_2Mo$: C, 49.54; H, 7.18. Found: C, 49.34; H, 7.15. μ_{eff} = 2.68 μ_B (Gouy balance). ^{1}H NMR (benzene-d_6, 300 MHz) δ[ppm] = *trans*-isomer: 144.85 (2H (C*H*)), 5.79 (38H (CH_3)); *cis*-isomer: 68.13 (2H, (C*H*)), 4.27 (18H, (CH_3)), 3.50 (18H (CH_3)). Ratio *trans*-isomer/*cis*-isomer in benzene-d_6 = 2.1:1.

2.1.3 Synthesis of [Mo(^{Ph}diket)$_2$Cl$_2$]

The title compound was prepared according to the general procedure described above from $MoCl_5$ (0.99 g, 3.63 mmol, 1.0 equiv.) and ^{Ph}diketH (2.41 g, 10.8 mmol, 3.0 equiv.), resulting in the formation of a dark black-grey micro-crystalline solid. Washing with large volumes of MeCN, THF, and Et_2O afforded [Mo(^{Ph}diket)$_2$Cl$_2$] of high enough purity for further investigations. Yield: 1.05 g (1.7 mmol, 47%). Anal. Calcd for $C_{30}H_{22}O_4Cl_2Mo$: C, 58.75; H, 3.62. Found: C, 58.34; H, 3.91. μ_{eff} = 2.72 μ_B (Gouy balance). ^{1}H NMR (MeCN-d_3, 300 MHz) δ[ppm] = *trans*-isomer: -39.75 (br, 2 C*H*), 0.70 (4 *para*-C*H*), 2.80 (8 *ortho*/*meta*-C*H*), 8.92 (8 *ortho*/*meta*-C*H*). For XRD-analysis, [Mo(^{Ph}diket)$_2$Cl$_2$] was recrystallized by slow diffusion of ^{n}pentane into a saturated pyridine solution. The complex was isolated as [Mo(^{Ph}diket)$_2$Cl$_2$(pyr)] (see Section S3 below for XRD analysis).

2.1.4 Attempted synthesis of [Mo(^{CF3}diket)$_2$Cl$_2$]

After refluxing [$MoCl_4$(MeCN)$_2$] in the presence of ^{CF3}diketH (3 equiv.) in MeCN for 14 h, a highly insoluble bright red precipitate was obtained. The formation of the target complex was suggested by ^{1}H NMR spectroscopy of the crude reaction mixture due to the presence of a characteristic signal for the methine C*H* proton of the coordinated diketonate ligand at δ = 155.70 ppm (Figure S1). Nevertheless, the presence of multiple peaks in the ^{19}F NMR spectrum of the same sample suggested the formation of a complex reaction mixture (Figure S2).
Recrystallization from CH_2Cl_2/^{n}pentane afforded a few red crystals, which were analyzed by single crystal XRD, identified as the co-crystallized decomposition species depicted in Figure S3 (CCDC deposition number: 2246899).

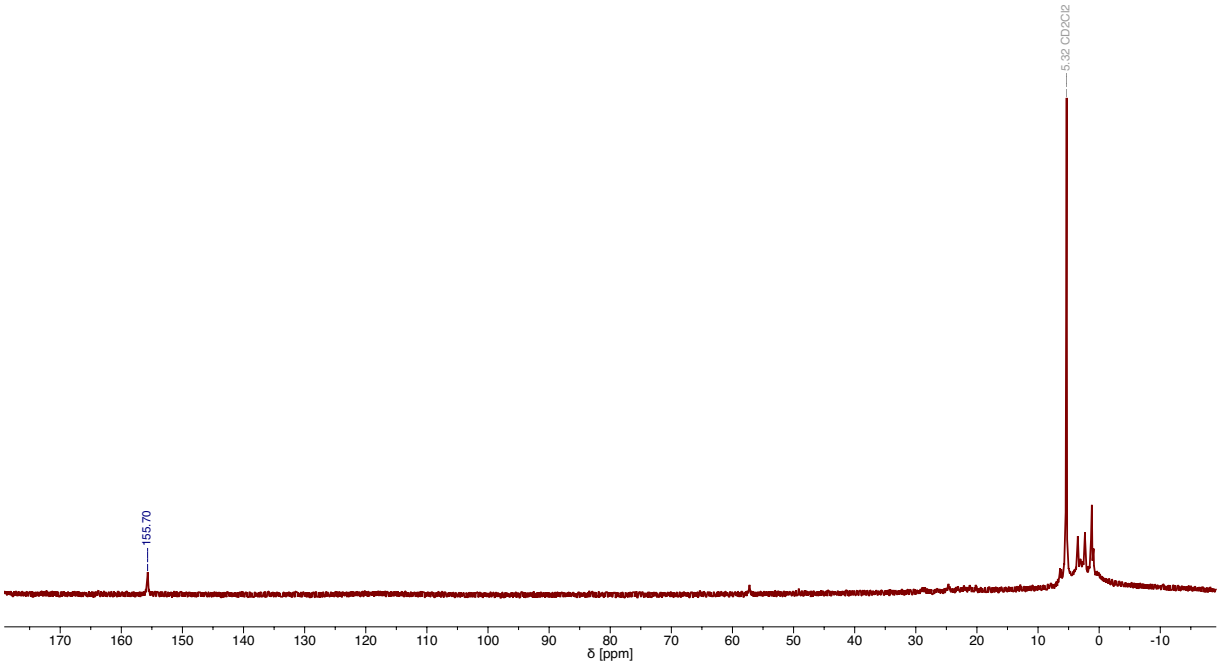

Figure S1: ^{1}H NMR spectrum in CD_2Cl_2 of the crude reaction mixture ([$MoCl_5$] + ^{CF3}diketH).

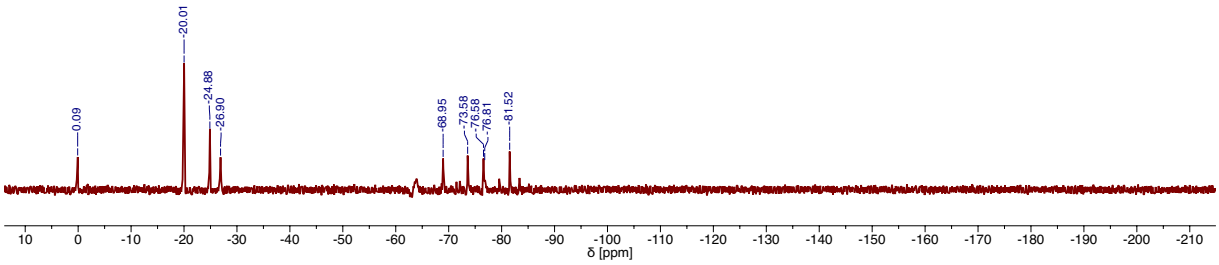

Figure S2: ^{19}F NMR spectrum in CD_2Cl_2 of the crude reaction mixture ([$MoCl_5$] + ^{CF3}diketH).

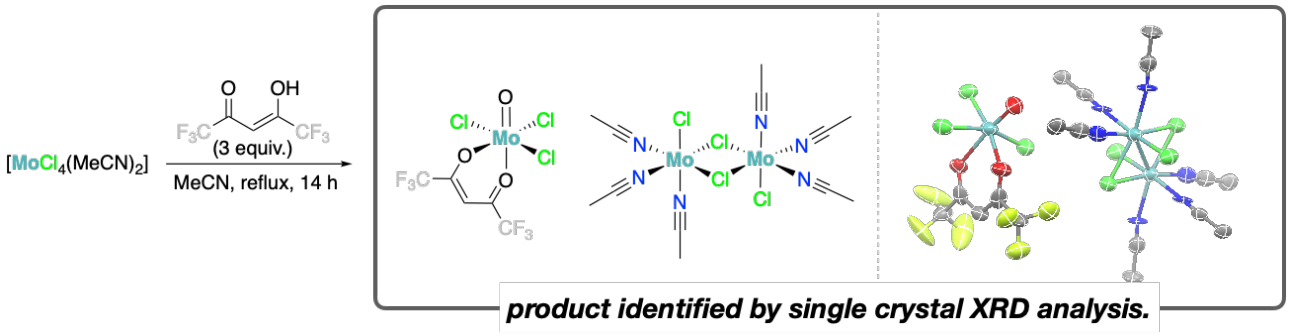

Figure S3: Reaction of [$MoCl_4(MeCN)_2$] with ^{CF3}diketH and corresponding product identified XRD analysis.

2.2 General Procedure for the preparation of [$Mo^{IV}(^{R}diket)_2(OTf)_2$] (diket = β-diketonate)

In a scintillation vial (20 mL), [$Mo(^{R}diket)_2Cl_2$] (1.00 equiv.) was dissolved/suspended in DME (10 mL). AgOTf (2.05 equiv.) was added as a solid and the reaction was stirred for three hours at room temperature. The formed AgCl salt (visible as a colorless precipitate) was centrifuged off and the filtrate was taken to dryness, affording crude [$Mo(^{R}diket)_2(OTf)_2$], whose properties depend on the present diketonate ligand. Further purification steps are described below for each complex.

2.2.1 Synthesis of [Mo(^{Me}diket)$_2$(OTf)$_2$]

The title compound was prepared according to the general procedure described above from [Mo(acac)$_2$Cl$_2$] (182 mg, 0.50 mmol, 1.0 equiv.) and AgOTf (270 mg, 1.05 mmol, 2.1 equiv.), resulting the formation of a dark red, sticky solid. This crude product was further purified by recrystallization from CH_2Cl_2/Et_2O at -35 °C, affording analytically pure [Mo(^{Me}diket)$_2$(OTf)$_2$]. Yield: 255 mg (0.43 mmol, 86%). Anal. Calcd for $C_{12}H_{14}F_6O_8S_2Mo$: C, 24.33; H, 2.38. Found: C, 24.27; H, 2.44. μ_{eff} = 2.70 μ_B (Evans Method, in C_6D_6). ^{1}H NMR (C_6D_6, 300 MHz) δ[ppm] = *trans*-isomer: 158.65 (2H (C*H*)), 108.13 (12H (CH_3)); *cis*-isomer: 131.83 (2 (C*H*)), 113.88 (3H (CH_3)), 101.75 (3H (CH_3)). Ratio *trans*-isomer/*cis*-isomer = 13:1. ^{19}F NMR (C_6D_6, 282 MHz) δ[ppm] = (*trans*-isomer: -40.05 (CF_3); *cis*-isomer: -43.49 (CF_3).

2.2.2 Synthesis of [Mo(^{tBu}diket)$_2$(OTf)$_2$]

The title compound was prepared according to the general procedure described above from [Mo(^{tBu}diket)$_2$Cl$_2$] (1.61 g, 3.0 mmol, 1.0 equiv.) and AgOTf (1.62 g, 6.3 mmol, 2.1 equiv.), resulting in the formation of a dark red solid. This crude product was further purified by recrystallization from MeCN at -35 °C, affording analytically pure [Mo(^{tBu}diket)$_2$(OTf)$_2$]. Yield: 1.93 g (2.53 mmol, 71.4%). Anal. Calcd for $C_{24}H_{38}F_6O_8S_2Mo$: C, 37.90; H, 5.04. Found: C, 38.00; H, 4.95. μ_{eff} = 2.76 μ_B (Gouy balance). μ_{eff} = 3.04 μ_B (Evans Method, in MeCN-d_3). ^{1}H NMR (benzene-d_6, 300 MHz) δ[ppm] = *trans*-isomer: 146.37 (2H (C*H*)), 4.96 (36 (CH_3)); *cis*-isomer: 147.51 (2H (C*H*)), 5.94 (18H (CH_3)), 5.71 (18H (CH_3)). Ratio *trans*-isomer/*cis*-isomer in benzene-d_6 = 1.9:1. ^{19}F NMR (benzene-d_6, 282 MHz) δ[ppm] = *trans*-isomer: -40.81 (2 CF_3); *cis*-isomer: -44.74 (2 CF_3). UV-Vis (0.25 mM in CH_2Cl_2): λ_{max} [nm] ([$10^3 \cdot M^{-1} \cdot cm^{-1}$]) = 241 (13.9), 271 (12.2, sh), 341 (5.5), 379 (4.5), 464 (2.5).

2.2.3 Synthesis of [Mo(^{Ph}diket)$_2$(OTf)$_2$]

The title compound was prepared according to the general procedure described above from [Mo(^{Ph}diket)$_2$Cl$_2$] (126 mg, 0.21 mmol, 1.0 equiv.) and AgOTf (116 mg, 0.45 mmol, 2.1 equiv.), resulting in the formation of a dark red solid. Because of inherently low solubility of the material in DME, THF was used for extraction. The filtrate was dried *in vacuo* immediately to prevent potential polymerization of THF. The solid was further purified by washing with MeCN (5 mL) followed by Et_2O (5 mL) affording analytically pure product.

Yield: 132 mg (0.16 mmol, 76%). Anal. Calcd for $C_{24}H_{38}F_6O_8S_2Mo$: C, 45.72; H, 2.64. Found: C, 45.90; H, 2.78. μ_{eff} = 2.71 μ_B (Evans Method, in CD_2Cl_2). ^{1}H NMR (CD_2Cl_2, 300 MHz) δ[ppm] = *trans*-isomer: 158.53 (2H (C*H*)), 13.60 (8 (C*H*)), -7.37 (8 (C*H*)), -11.60 (4 (C*H*)); *cis*-isomer: 152.54 (2H (C*H*)), 14.51 (4H (C*H*)), 13.73 (4H (C*H*)), -7.93 (4H (C*H*)), -10.29 (4H (C*H*)), -13.08 (2H (C*H*)), -15.21 (2H (C*H*)). Ratio *trans*-isomer/*cis*-isomer in CD_2Cl_2 = 1:7.3. ^{19}F NMR (CD_2Cl_2, 282 MHz) δ[ppm] = *trans*-isomer: -39.30 (2 CF_3); *cis*-isomer: -44.68 (2 CF_3). Single crystals suitable for XRD analysis were grown by slow diffusion of diethyl ether into a saturated solution in dichloromethane at -35 °C (see Section S3 below for XRD analysis).

2.3 Synthesis of [Mo^{V}(O)(^{tBu}diket)$_2$(OTf)]

The title compound was prepared by salt metathesis between [Mo(^{tBu}diket)$_2$Cl$_2$] (300 mg, 0.56 mmol, 1.0 equiv.) and AgOTf (304 mg, 1.18 mmol, 2.2 equiv.) in a 3:1 mixture of THF/Et_2O (V_{tot} = 10 mL), stirred at room temperature for 25 min. The formed AgCl was removed as a colorless precipitate by centrifugation. H_2O (50 μL, 2.78 mmol, 5.0 equiv.) was added and the mixture was stirred overnight. The color changed slowly from red/orange to brown. All volatiles were removed under reduced pressure affording a dark purple oil. After trituration with MeCN (10 mL), a green crystalline solid was obtained. The crude product was further recrystallized from MeCN at -35 °C, affording the target compound as a bright green crystalline solid. Yield (only the 1st fraction was collected): 108 mg (0.17 mmol, 31%). Anal. Calcd for $C_{23}H_{38}F_3O_8SMo$: C, 44.02; H, 6.10. Found: C, 44.00; H, 6.15. ^{1}H NMR (benzene-d_6, 300 MHz) δ[ppm] = 2.50 (38H (CH_3), br). ^{19}F NMR (benzene-d_6, 282 MHz) δ[ppm] = -76.99 (CF_3). UV-Vis (0.25 mM in CH_2Cl_2): λ_{max} [nm] ([$10^3 \cdot M^{-1} \cdot cm^{-1}$]) = 266 (14.0), 352 (6.4).

2.4 Synthesis of [Mo^{VI}(N)(^{tBu}diket)$_2$(OTf)]

Neat $TMSN_3$ (82 μL, 0.64 mmol, 1.2 equiv.) was added to a solution of [Mo(^{tBu}diket)$_2$(OTf)$_2$] (400 mg, 0.52 mmol, 1.0 equiv.) in CH_2Cl_2 (8 mL) and the resulting mixture was stirred for 3 h at room temperature. The color changed from bright red to dark brown/black. All volatiles were removed under reduced pressure affording a dark powder. The crude product was further purified by washing with cold ^{n}pentane (2 mL) followed by recrystallization from Et_2O at -35 °C, affording the target complex as black crystalline blocks. Yield (in two fractions): 261 mg (0.42 mmol, 80%). Anal. Calcd for $C_{23}H_{38}F_3NO_7SMo$: C, 44.16; N, 2.24; H, 6.12. Found: C, 44.33; N, 2.28; H, 6.09.

2.5 Reaction of [Mo(^{tBu}diket)$_2$Cl$_2$] with AgSbF$_6$

Aiming at synthetizing [Mo^{VI}(^{tBu}diket)$_2$][SbF$_6$]$_2$, we applied the procedure described in Section 2.2 using [Mo(^{tBu}diket)Cl$_2$] and substituting AgOTf with AgSbF$_6$. While we were unable to isolate the desired complex, several products were identified by single crystal XRD analysis, as depicted in Figure S4. None of the complexes have been quantified or further analyzed.

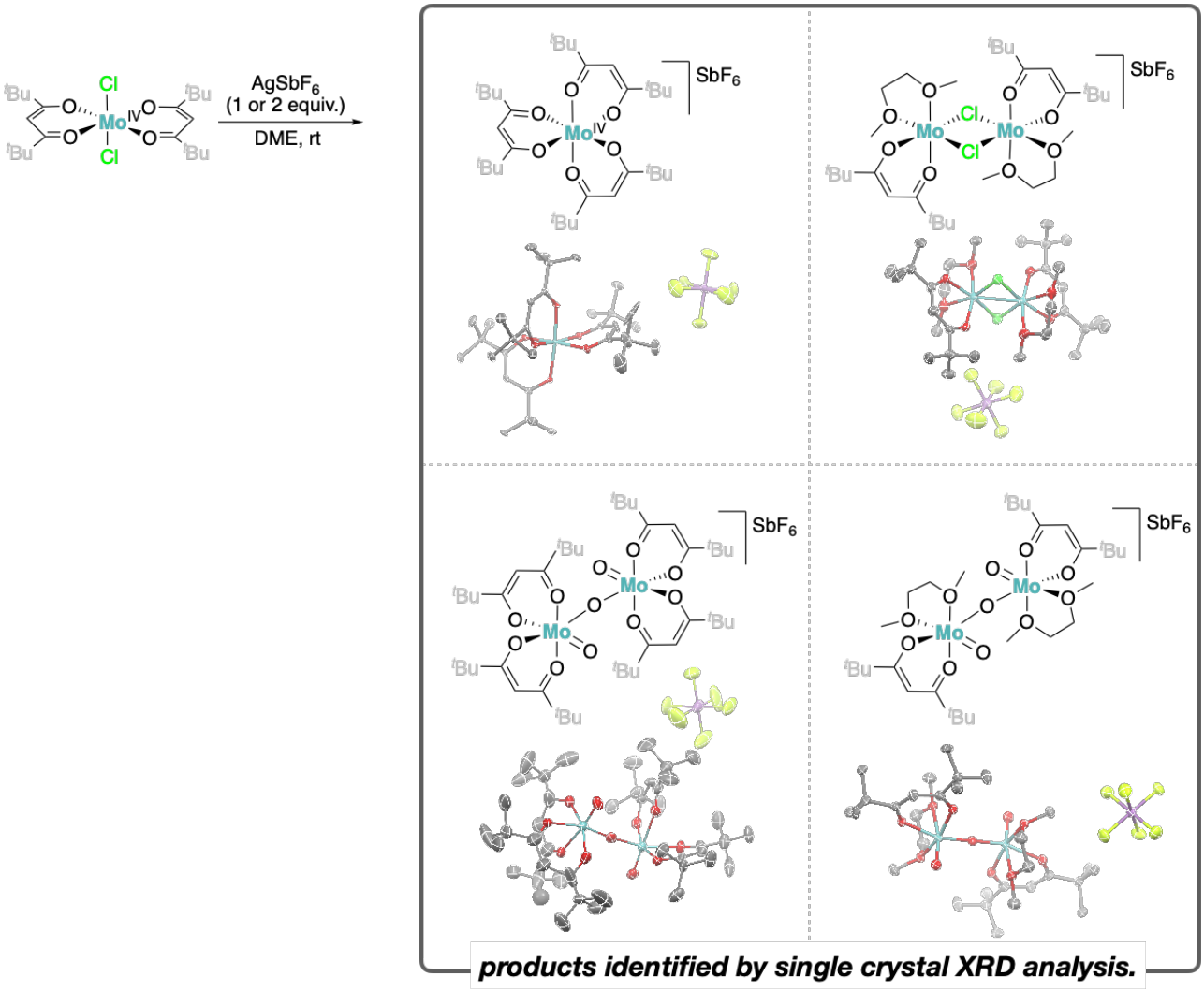

Figure S4: Reaction of [Mo(^{tBu}diket)$_2$Cl$_2$] with AgSbF$_6$.

3. Catalytic Tests

3.1 General Procedure

Standard catalytic tests were run in 20 mL finger shaped Schlenk flasks. The substrates (1 mmol) were dissolved in CH_2Cl_2 (5 mL). A solution of the [Mo]-catalyst (and additive) in CH_2Cl_2 (5 mL) was prepared in a separate Schlenk flask and added to the substrate solution by syringe, while stirring. The reaction was monitored by TLC and upon completion, the mixture was filtered through a short pad of silica. All volatiles were removed under reduced pressure and the crude was purified by flash column chromatography using mixtures of hexane/ethyl acetate as eluent. If the product is not

isolated, ^{1}H NMR yields are reported using CH_2Br_2 as internal standard. Spectra of isolated products were identical to previous literature reports.

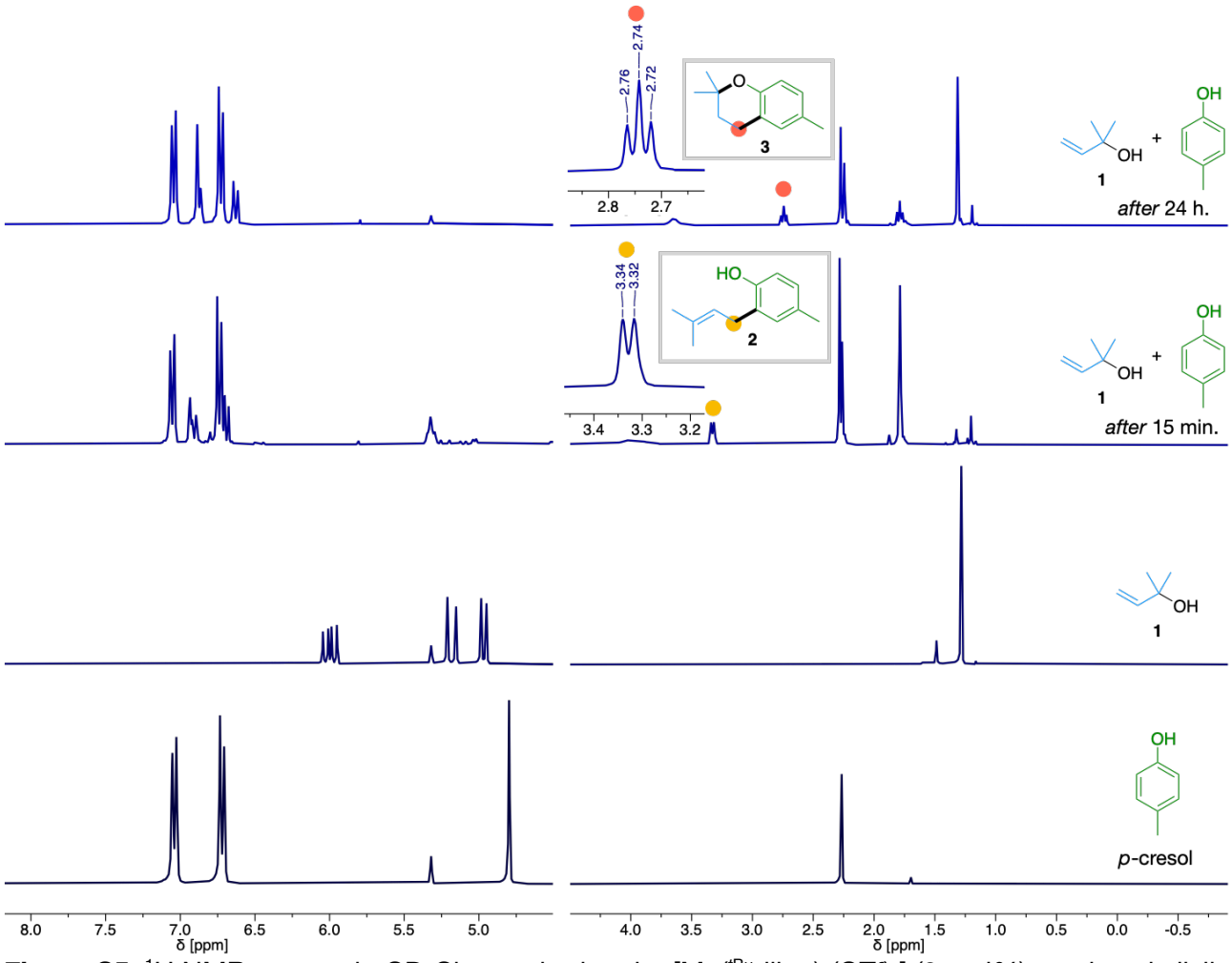

Figure S5: ^{1}H NMR spectra in CD_2Cl_2, monitoring the [Mo(^{tBu}diket)$_2$(OTf)$_2$] (2 mol%) catalyzed allylic substitution of allylic alcohol **1** (1.0 equiv.) with *p*-cresol (1.3 equiv.) (in CD_2Cl_2, room temperature, *after* 15 min. and 24 h). Spectral assignments of intermediate **2**,[2] and product **3**,[3] are in full agreement with literature.

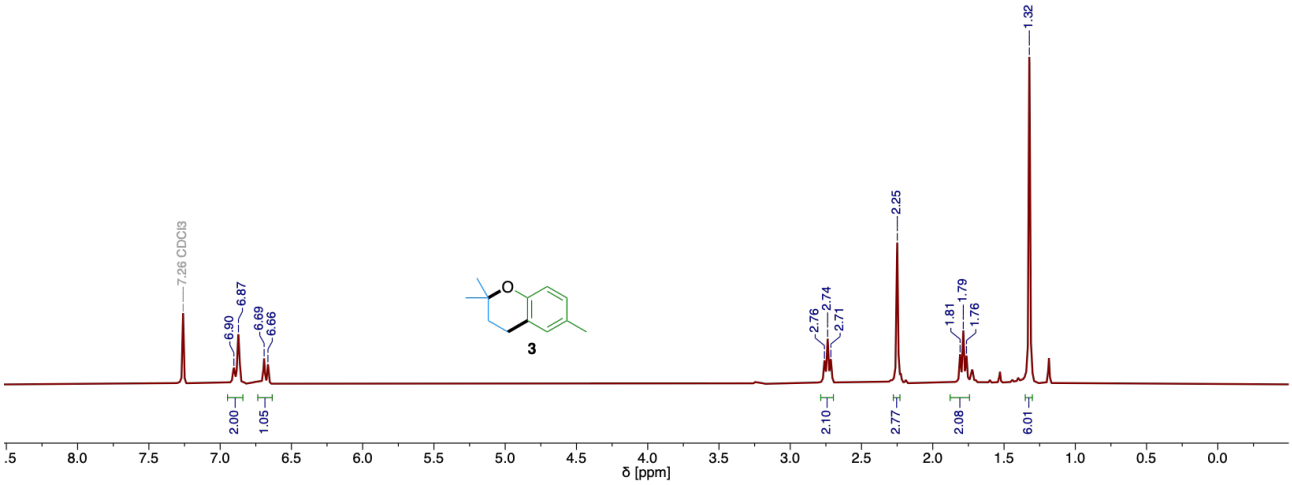

Figure S6: ^{1}H NMR of product **3** (isolated by flash column chromatography 0-3% EtOAc/^{n}hexane) in $CDCl_3$. Reaction conditions: [Mo(^{tBu}diket)$_2$(OTf)$_2$] (2 mol%) allylic alcohol **1** (1.0 equiv.) with *p*-cresol (1.3 equiv.), in CH_2Cl_2, room temperature 24 h).

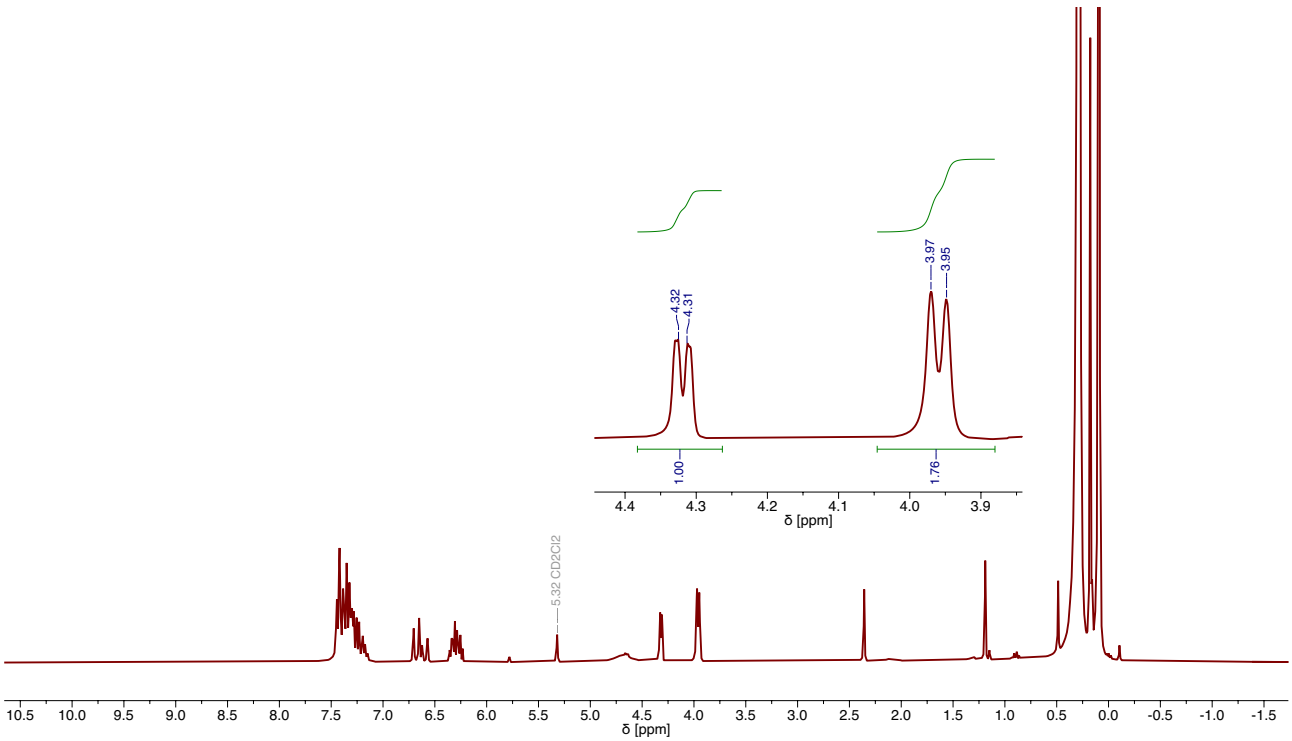

Figure S7: ^{1}H NMR spectrum in in CD_2Cl_2 of the allylic substitution of cinnamyl alcohol (1 equiv.) with trimethylsilyl azide (10 equiv.), catalyzed by [Mo(^{tBu}diket)$_2$(OTf)$_2$] (2 mol%) (room temperature, after 15 min). The conversion was determined from relative integration of allylic proton signals of product ((*E*)-cinnamyl azide, δ = 3.97, 3.95 ppm) *vs.* starting material (cinnamyl alcohol, δ = 4.32, 4.31 ppm).

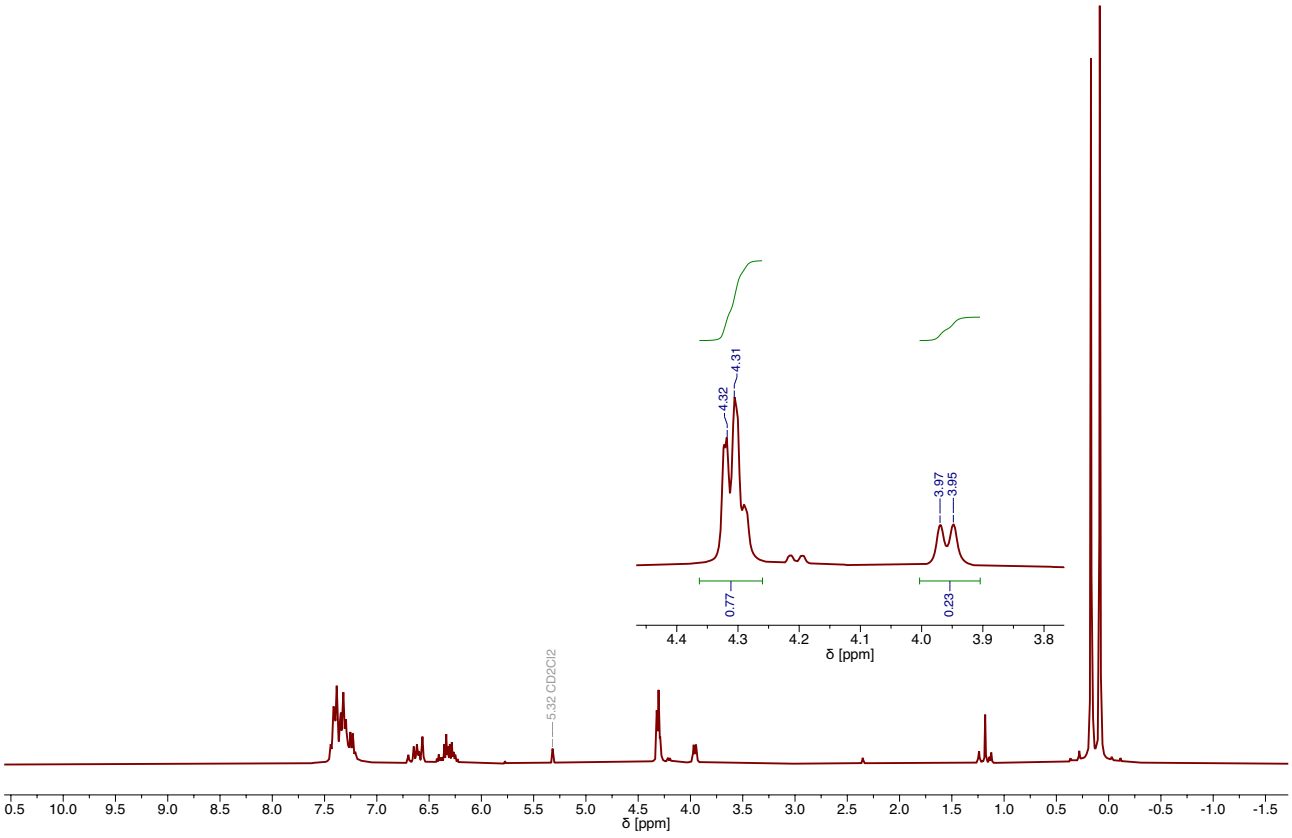

Figure S8: ^{1}H NMR spectrum in in CD_2Cl_2 of the allylic substitution of cinnamyl alcohol (1 equiv.) with trimethylsilyl azide (1.2 equiv.), catalyzed by [Mo(N)(^{tBu}diket)$_2$(OTf)] (2 mol%) (room temperature, after 30 min). The conversion (= 22%) was determined from relative integration of allylic proton signals of product ((*E*)-cinnamyl azide, δ = 3.97, 3.95 ppm) *vs.* starting material (cinnamyl alcohol, δ = 4.32, 4.31 ppm).

3.2 Kinetic Analysis

The experiments were set up as described in Section 3.1. Aliquots of 0.7 mL were sampled from the solution and immediately filtered through a short plug of silica. The plug of silica was washed with at least five column volumes of CH_2Cl_2. All volatiles were removed under reduced pressure and the remaining oil was dissolved in a stock solution (0.1 M CH_2Br_2 in $CDCl_3$) of exact volume (typically 0.7 mL). Yields were determined by ^{1}H NMR (300 MHz, 16 scans, D_1 = 10 s) using the CH_2Br_2 signal (δ = 4.93 ppm, CH_2) as an internal standard and the signals of the methylene protons of the coupled products, (*E*)-4-cinnamylphenol and (*E*)-2-cinnamylphenol (*see* Scheme S1 for details).[4] The conversion was calculated according to equation (1):

$$conversion(in\%) = 100 \times \frac{n_{para} + n_{ortho}}{n_{cinnamylalcohol}} \quad (1)$$

, where n_{para} and n_{ortho} are the yields (in mmol) of *para*- and *ortho* coupled products, and $n_{cinnamyl\ alcohol}$ is the amount (in mmol) of cinnamyl alcohol starting material used (typically 1 mmol). For the catalytic tests carried out in CD_2Cl_2, aliquots (V = 1 mL) were sampled from the reaction mixture and filtered through a plug of silica. Conversion was determined by ^{1}H NMR spectroscopy.

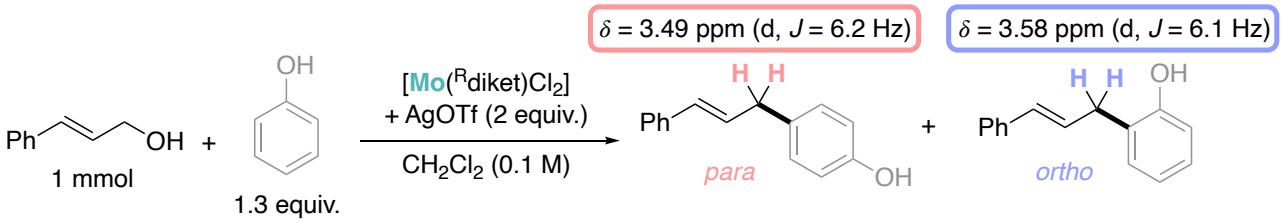

Scheme S1: Prototypical catalytic reaction conditions used for kinetic investigations. The indicated chemical shifts were used, in combination with the signal of the internal standard CH_2Br_2 (δ = 4.93 ppm), to determine yields and conversion after specific reaction times.

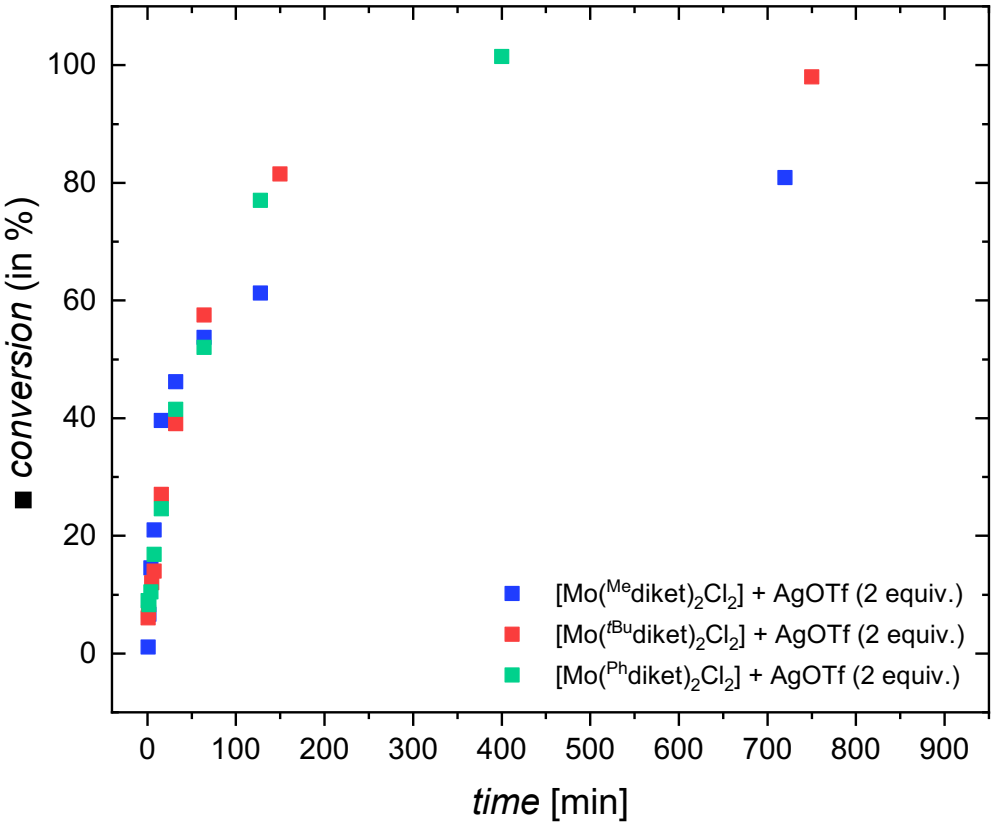

Figure S9: Conversion *vs.* time plot for the allylic substitution of cinnamyl alcohol (1.0 equiv.) with phenol (1.3 equiv.), catalyzed by [Mo(^{R}diket)$_2$Cl$_2$] (0.5 mol%) (R = Me (*blue*), ^{t}Bu (*red*), Ph (*green*)) in the presence of AgOTf (1 mol%) (CH_2Cl_2, room temperature). Conversion was followed by ^{1}H NMR spectroscopy.

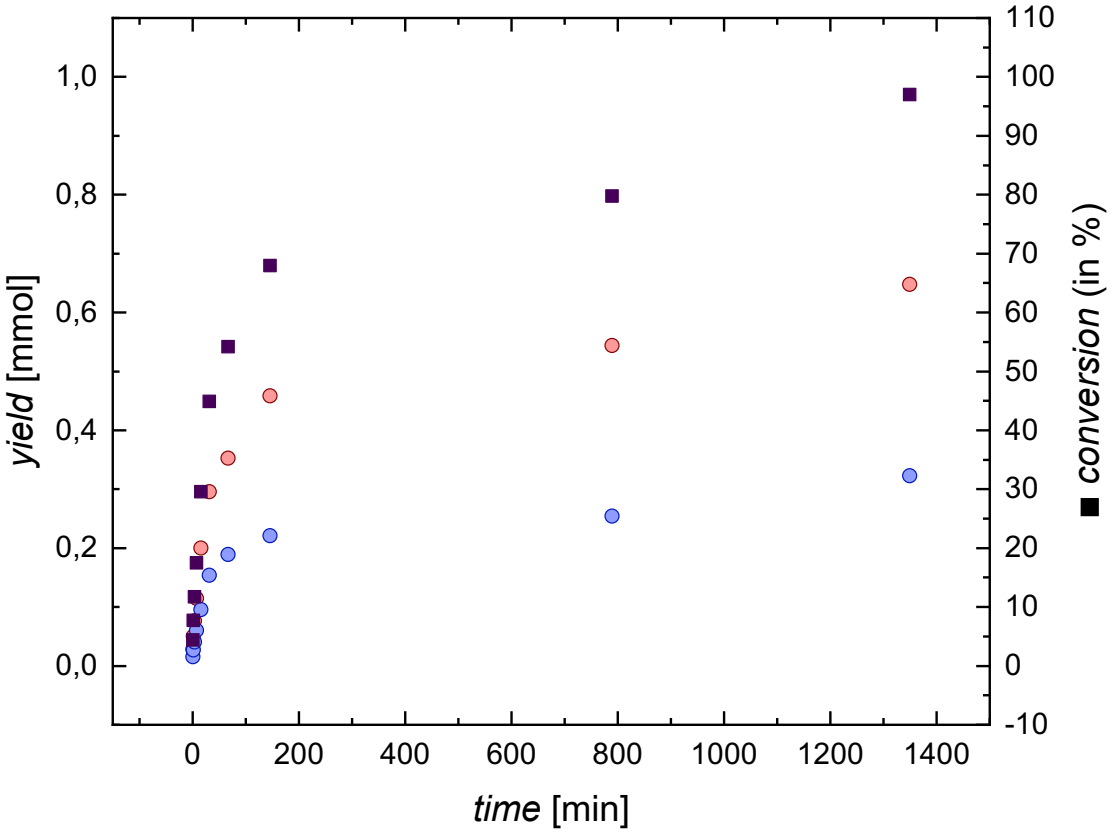

Figure S10: Conversion *vs.* time plot for the allylic substitution of cinnamyl alcohol (1.0 equiv.) with phenol (1.3 equiv.), catalyzed by [Mo(^{tBu}diket)$_2$(OTf)$_2$] (0.5 mol%) (CH_2Cl_2, room temperature).

Conversion was followed by ^{1}H NMR spectroscopy. *Pink* dots: conversion of (*E*)-4-cinnamylphenol; *blue* dots: of (*E*)-2-cinnamylphenol; *purple* squares: combined conversion.

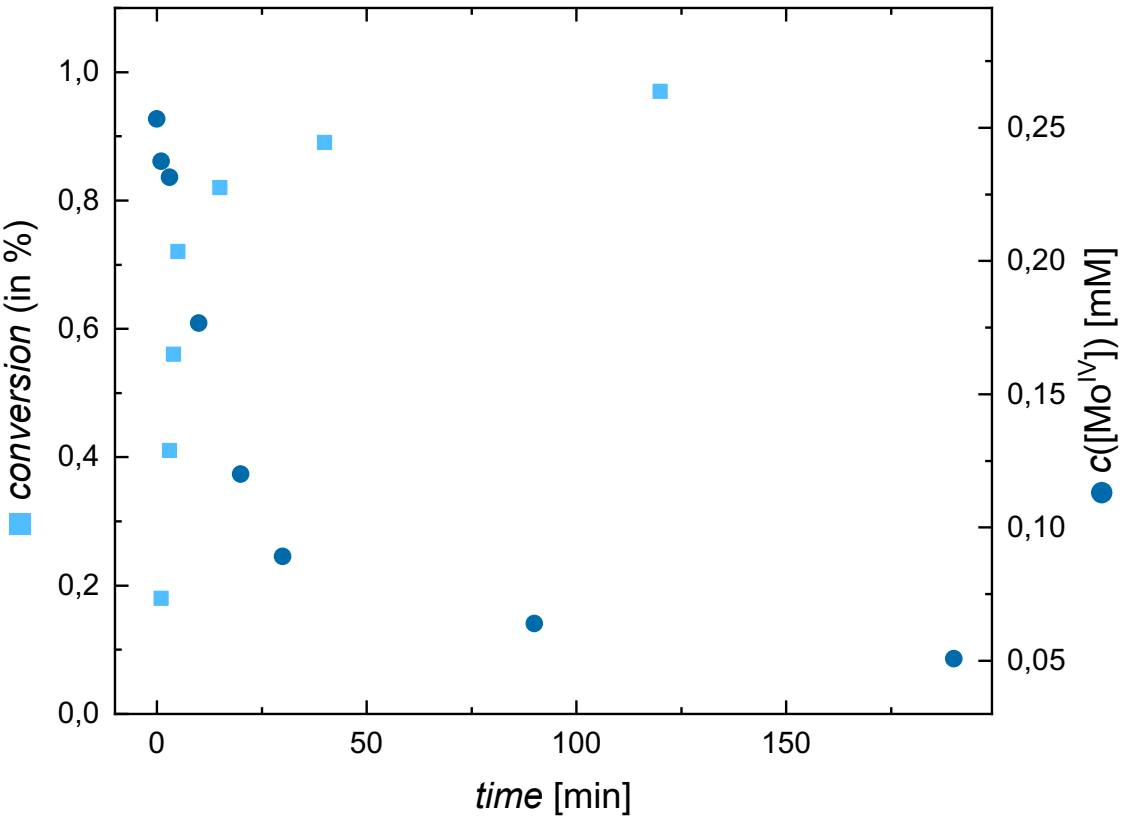

Figure S11: Conversion *vs.* time plot for the allylic substitution of cinnamyl alcohol (1.0 equiv.) with phenol (1.3 equiv.), catalyzed by [Mo($^{t\text{Bu}}$diket)$_2$(OTf)$_2$] (1 mol%) (CD_2Cl_2, room temperature). Product formation was followed by ^{1}H NMR spectroscopy. The concentration of [Mo($^{t\text{Bu}}$diket)$_2$(OTf)$_2$] ([Mo^{IV}]) was determined by UV-Vis spectroscopy (absorption at λ = 500 nm (*vide infra*)).

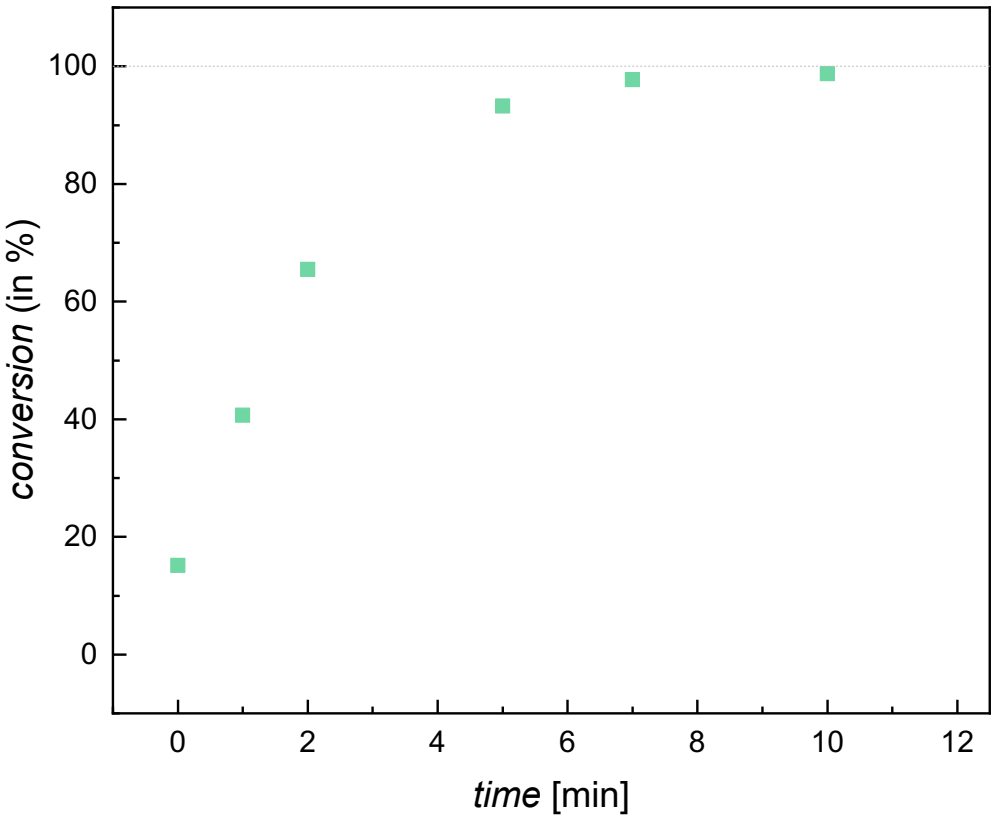

Figure S12: Conversion *vs.* time plot for the allylic substitution of cinnamyl alcohol (1.0 equiv.) with phenol (1.3 equiv.), catalyzed by [Mo($^{t\text{Bu}}$diket)$_2$(OTf)$_2$] (1 mol%), in presence of activated 4 Å MS (CD_2Cl_2, room temperature). Conversion was followed by ^{1}H NMR spectroscopy.

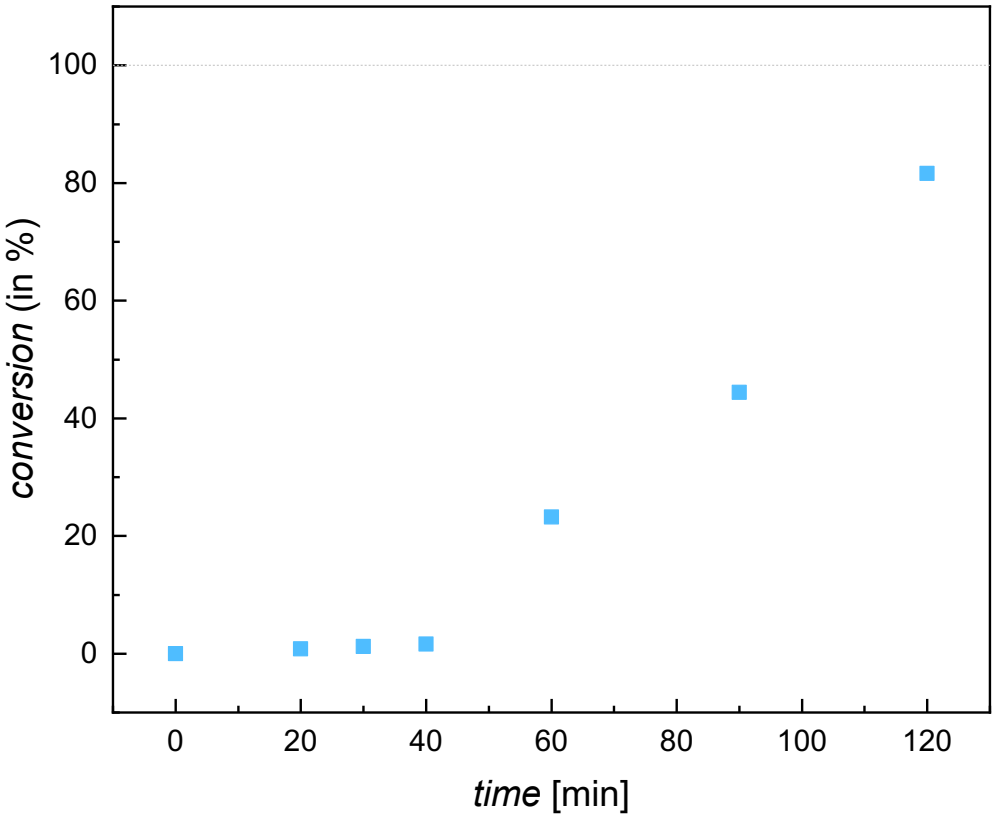

Figure S13: Conversion *vs.* time plot for the allylic substitution of cinnamyl alcohol (1.0 equiv.) with phenol (1.3 equiv.), catalyzed by [Mo(O)($^{t\text{Bu}}$diket)$_2$(OTf)] (1 mol%) (CD_2Cl_2, room temperature). Conversion was followed by ^{1}H NMR spectroscopy.

3.3 Mechanistic Studies

3.3.1 *In-Situ* UV-Vis Study

The catalytic reaction was monitored by UV-Vis spectroscopy using a dip probe connected by an optical fiber to a UV-Vis spectrometer (d = 2 mm), inside a glove box.

In a typical experiment, phenol (0.130 mmol, 1.3 equiv.) and [Mo($^{t\text{Bu}}$diket)$_2$(OTf)$_2$] (0.001 mmol, 1 mol%) were dissolved in CH_2Cl_2 (4 mL) in a scintillation vial (20 mL). The UV-Vis dip probe was introduced into the solution though a septum. The reaction was initiated by addition of allylic alcohol (0.100 mmol, 1.0 equiv.). UV-Vis spectra were recorded while constantly stirring at 280 rpm.

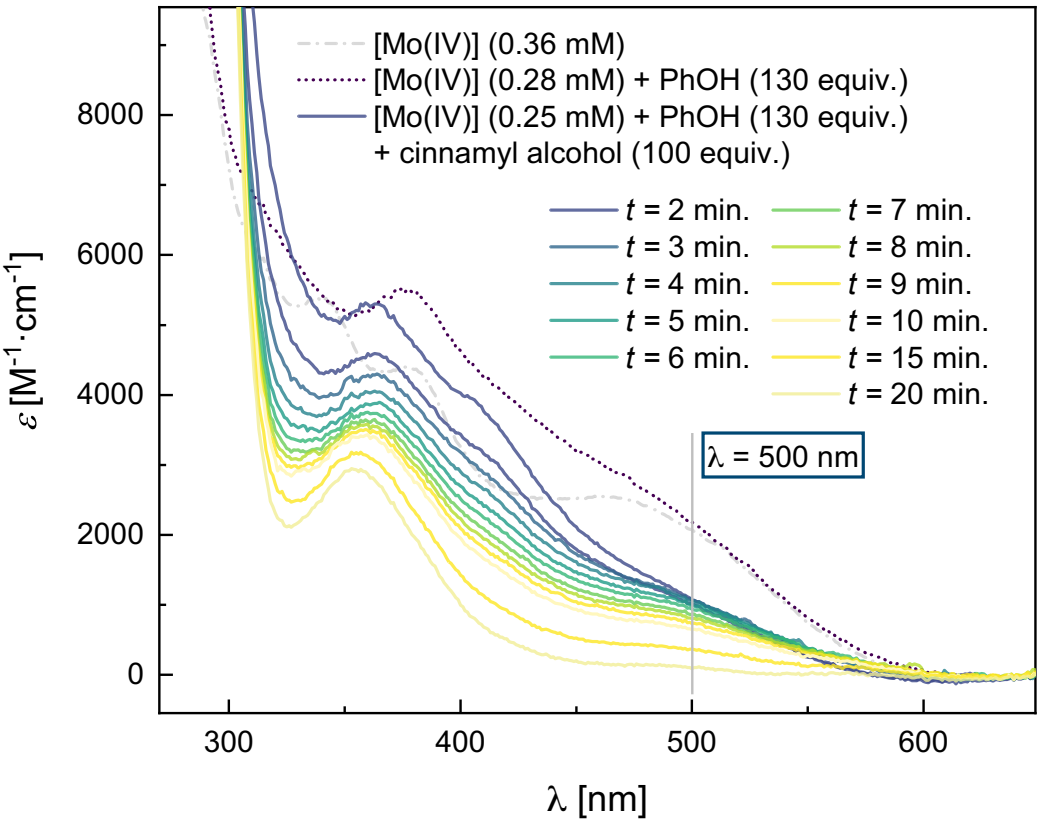

Figure S14: Time-dependent UV-Vis spectra recorded *in-situ* for the allylic substitution of cinnamyl alcohol (1.0 equiv.) with phenol (1.3 equiv.) catalyzed by [Mo($^{t\text{Bu}}$diket)$_2$(OTf)$_2$] (1 mol%) (CD_2Cl_2, room temperature).

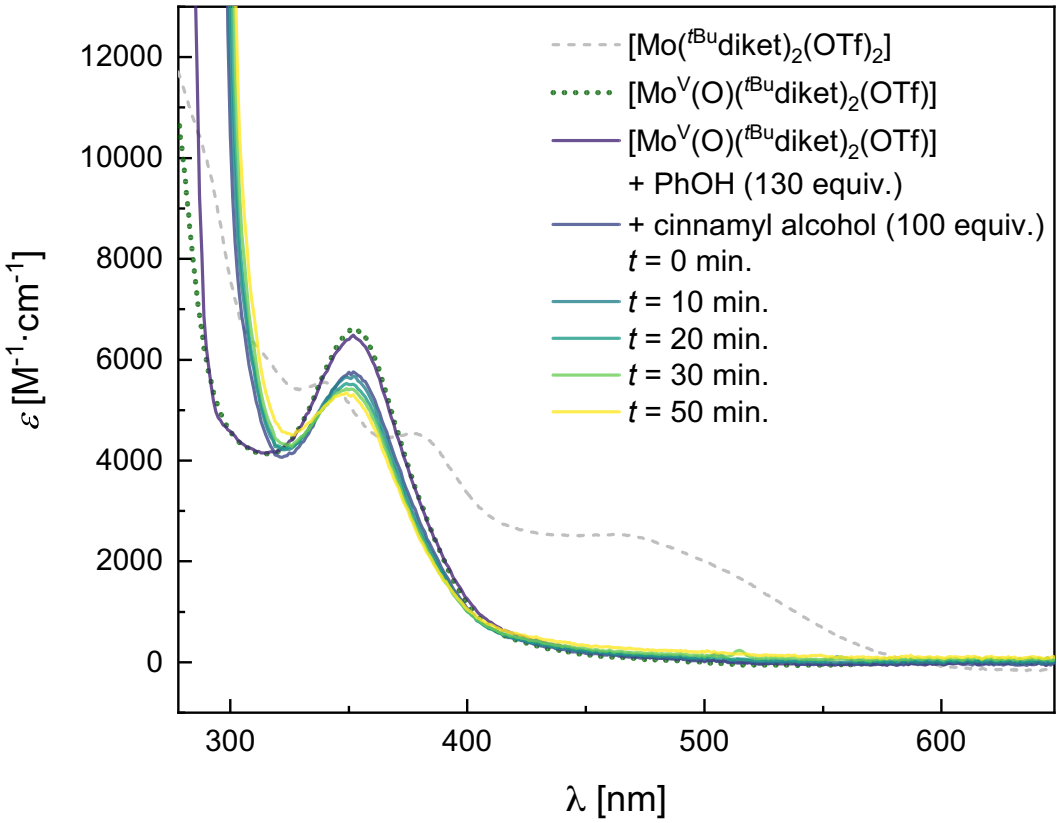

Figure S15: Time-dependent UV-Vis spectra recorded *in-situ* for the allylic substitution of cinnamyl alcohol (1.0 equiv.) with phenol (1.3 equiv.) catalyzed by [Mo(O)($^{t\text{Bu}}$diket)$_2$(OTf)] (1 mol%) (CD_2Cl_2, room temperature).

3.3.1 Stoichiometric Reactivity Tests Followed by ^{1}H NMR Spectroscopy

The two substrates, cinnamyl alcohol (*green*) and phenol (*dark blue*), were analyzed by ^{1}H NMR. No background reaction was observed in 1:1 mixtures (*magenta*).

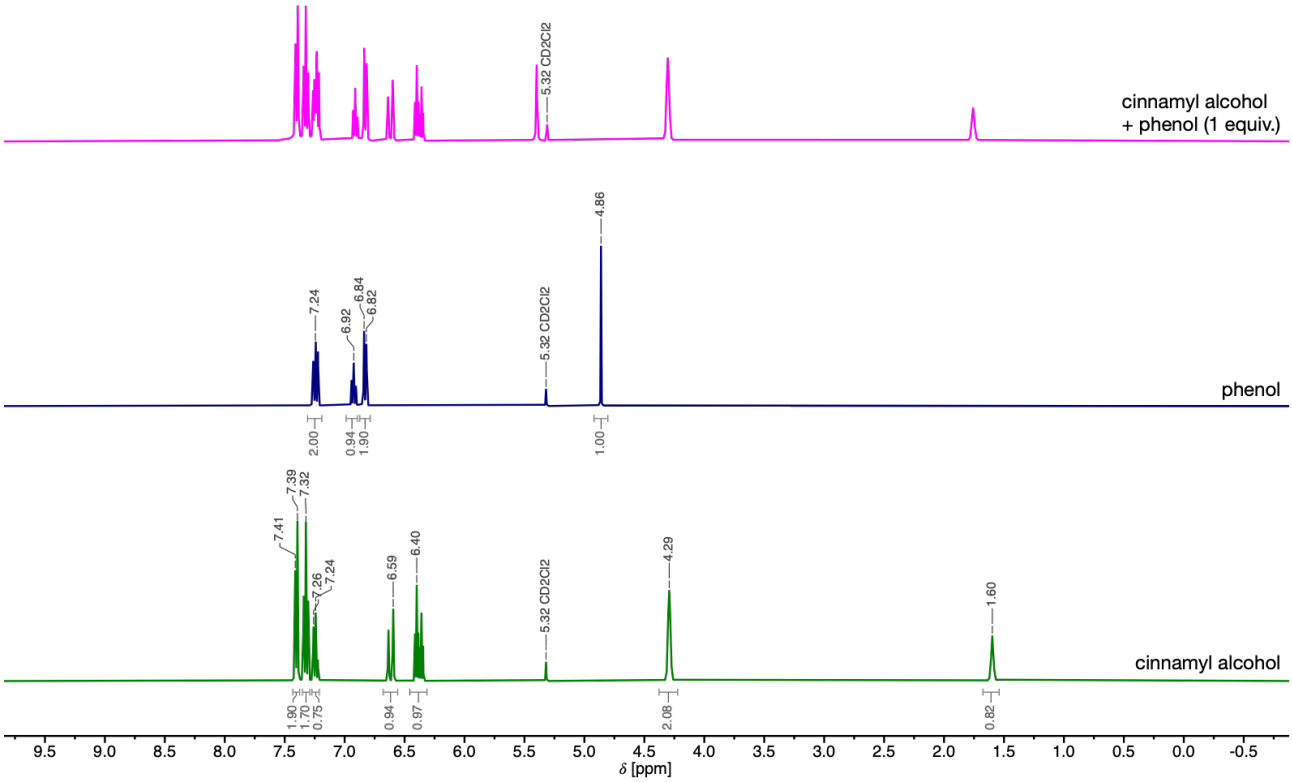

Figure S16: ^{1}H NMR spectra of cinnamyl alcohol (**1**, *green*), phenol (**2**, *dark blue*) and a 1:1 mixture of the two substrates (*magenta*) in CD_2Cl_2.

The reactivity of the [Mo($^{t\text{Bu}}$diket)$_2$(OTf)$_2$] with both substrates, cinnamyl alcohol and/or phenol, was investigated separately. In summary, we have found that the metal complex does not interact with phenol (*dark blue* spectrum in Figure S13, no spectral changes), whereas it reacts with cinnamyl alcohol under the formation of [Mo(O)($^{t\text{Bu}}$diket)$_2$(OTf)] (δ = 2.65 ppm, *magenta* spectrum in Figure S13 and Figure S14).

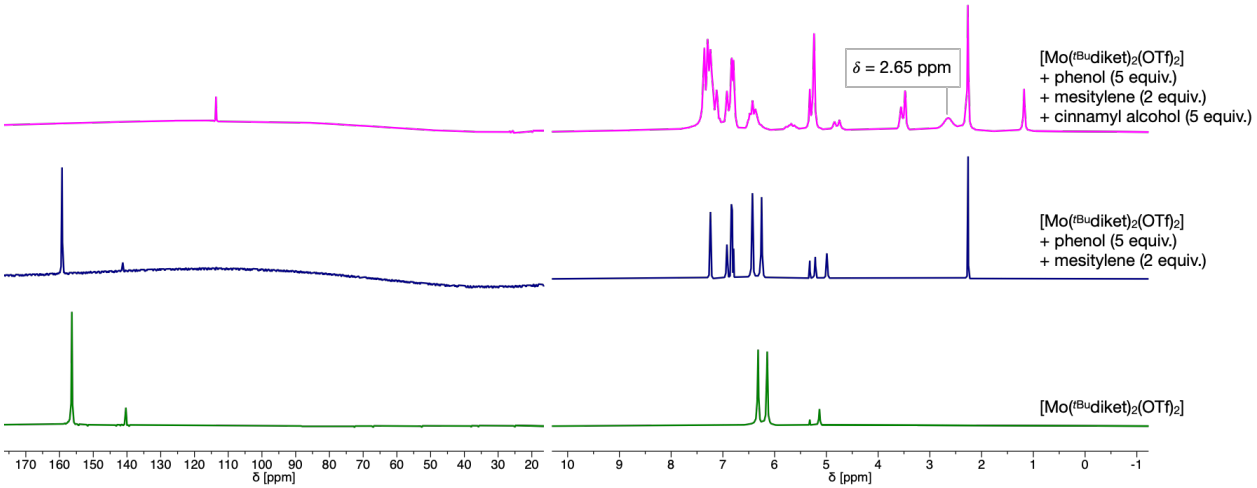

Figure S17: ^{1}H NMR spectra in CD_2Cl_2 probing the reactivity of [Mo($^{t\text{Bu}}$diket)$_2$(OTf)$_2$] (*green*) with phenol (*dark blue*) and additionally with cinnamyl alcohol (*magenta*). Mesitylene was added as a standard for quantitative comparison of the spectra.

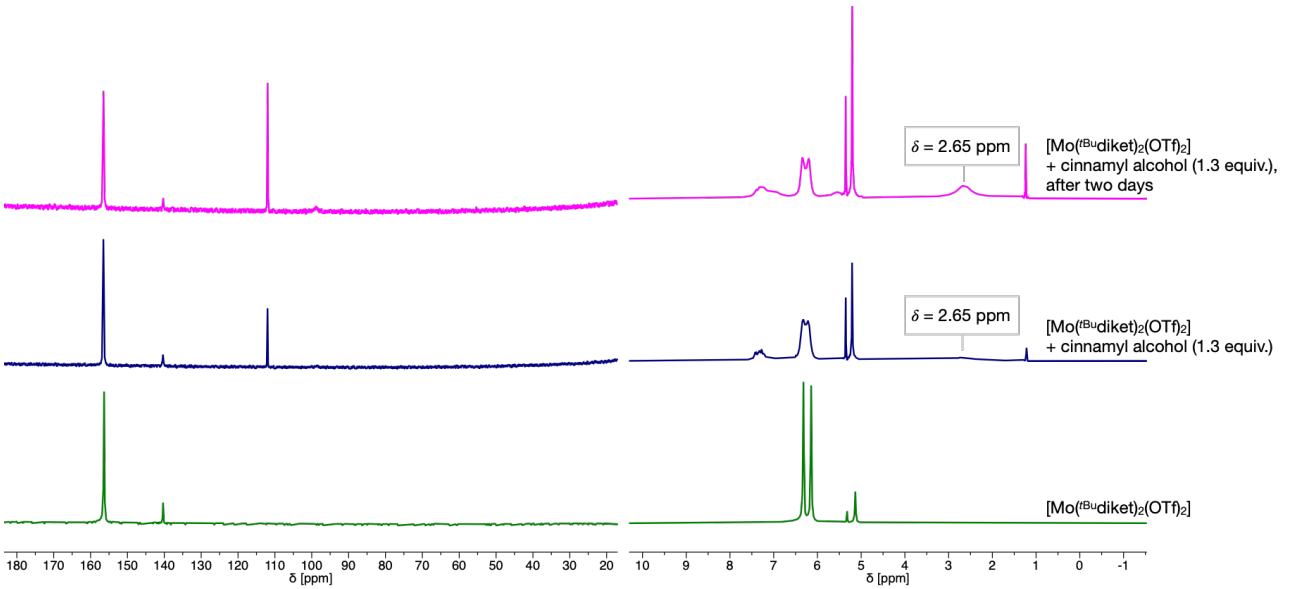

Figure S18: ^{1}H NMR spectra in CD_2Cl_2 probing the reactivity of [Mo($^{t\text{Bu}}$diket)$_2$(OTf)$_2$] (*green*) with cinnamyl alcohol (*dark blue*). The same spectrum was recorded again after two days standing in the NMR tube (*magenta*).

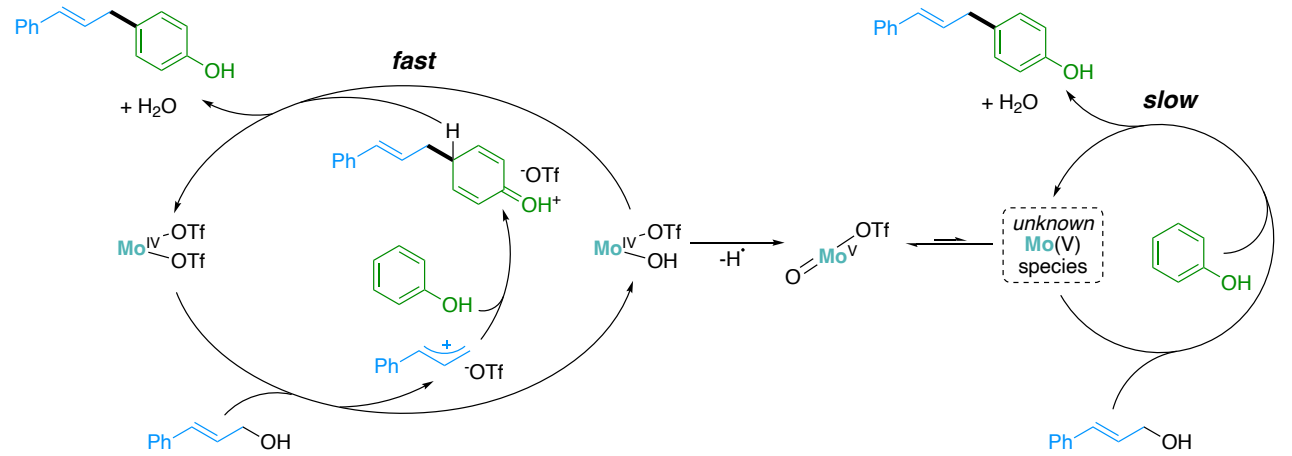

Scheme S2: Proposed catalytic cycles involving both the Mo(IV)- and the Mo(V) species.

4. XRD Data

4.1 General Procedure

Single crystals of structurally characterized compounds were grown as described in Section S2. Suitable crystals were selected under the atmosphere of an argon filled glove box and tip-mounted on a Rigaku R-AXIS SPIDER IP or Bruker APEX-II CCD diffractometer. The crystals were kept at 100 K during data collection. Using Olex2,[5] the structure was solved with the ShelXT[6] structure solution program using Intrinsic Phasing and refined with the SHELXL[7] refinement package using Least Squares minimization.

4.2 Refinement Details

Table S4: Refinement details of crystal structures of chloride complexes [Mo($^{\text{Me}}$diket)$_2$Cl$_2$], [Mo($^{t\text{Bu}}$diket)$_2$Cl$_2$], [Mo($^{\text{Ph}}$diket)$_2$Cl$_2$(pyr)] and [Mo(O)($^{\text{CF3}}$diket)Cl$_3$][{MoCl(μ-Cl)(MeCN)$_3$}$_2$].

Compound	[Mo($^{\text{Me}}$diket)$_2$Cl$_2$]	[Mo($^{t\text{Bu}}$diket)$_2$Cl$_2$]	[Mo($^{\text{Ph}}$diket)$_2$Cl$_2$(pyr)]	[Mo(O)($^{\text{CF3}}$diket)Cl$_3$] [{MoCl(μ-Cl)(MeCN)$_3$}$_2$]
Empirical formula	$C_{10}H_{14}Cl_2MoO_4$	$C_{24}H_{41}Cl_2MoNO_4$	$C_{35}H_{27}Cl_2MoNO_4$	$C_{11}H_{10}Cl_5F_6Mo_2N_3O_3$
Formula weight	365.05	574.42	692.41	715.35

Temperature [K]	100.0	100.0	100.0	100.00(13)
Crystal system	triclinic	monoclinic	monoclinic	triclinic
Space group	P-1	$P2_1/n$	$P2_1/c$	P-1
a [Å]	7.2362(5)	10.9632(5)	14.6472(5)	8.5740(3)
b [Å]	7.3583(5)	18.9755(7)	18.5664(6)	11.9059(5)
c [Å]	7.9687(6)	13.6819(6)	11.5099(3)	12.7345(5)
α [°]	92.355(3)	90	90	108.110(4)
β [°]	112.501(3)	92.743(2)	104.7610(10)	106.961(4)
γ [°]	118.207(3)	90	90	98.858(3)
Volume [Å^3]	332.36(4)	2843.0(2)	3026.77(16)	1138.21(8)
Z	1	4	4	2
ρ_{calc}g [cm^3]	1.824	1.342	1.519	2.087
μ [mm^{-1}]	1.387	0.676	0.651	15.079
F(000)	182.0	1200.0	1408.0	688.0
Crystal size [mm^3]	0.196 × 0.154 × 0.108	0.368 × 0.15 × 0.0154	0.377 × 0.122 × 0.093	0.152 × 0.056 × 0.043
Radiation	MoKα (λ = 0.71073)	MoKα (λ = 0.71073)	MoKα (λ = 0.71073)	Cu Kα (λ = 1.54184)
2Θ range for data collection [°]	5.752 to 54.924	5.126 to 50.698	4.266 to 54.206	11.11 to 122.334
Index ranges	-9 ≤ h ≤ 9, -9 ≤ k ≤ 9, -10 ≤ l ≤ 10	-13 ≤ h ≤ 13, 0 ≤ k ≤ 22, 0 ≤ l ≤ 16	-18 ≤ h ≤ 18, -23 ≤ k ≤ 23, -14 ≤ l ≤ 14	-8 ≤ h ≤ 9, -13 ≤ k ≤ 13, -13 ≤ l ≤ 14
Reflections collected	7118	5259	84193	8015
Independent reflections	1496 [R_{int} = 0.0198, R_{sigma} = 0.0174]	5259 [R_{int} = 0.0529, R_{sigma} = 0.0303]	6686 [R_{int} = 0.0390, R_{sigma} = 0.0165]	3406 [R_{int} = 0.0474, R_{sigma} = 0.0498]
Data/restraints/parameters	1496/0/81	5259/12/306	6686/0/388	3406/36/302
Goodness-of-fit on F^2	1.195	1.191	1.046	1.045
Final R indexes [I>=2σ (I)]	R_1 = 0.0220, wR_2 = 0.0530	R_1 = 0.0626, wR_2 = 0.1231	R_1 = 0.0224, wR_2 = 0.0500	R_1 = 0.0533, wR_2 = 0.1421
Final R indexes [all data]	R_1 = 0.0224, wR_2 = 0.0532	R_1 = 0.0825, wR_2 = 0.1377	R_1 = 0.0279, wR_2 = 0.0542	R_1 = 0.0627, wR_2 = 0.1488
Largest diff. peak/hole [e Å^{-3}]	0.65/-0.53	0.95/-0.77	0.43/-0.51	1.68/-0.74

Table S5: Refinement details of crystal structures of triflate complexes [Mo(^{Me}diket)$_2$(OTf)$_2$], [Mo(^{tBu}diket)$_2$(OTf)$_2$], and [Mo(^{Ph}diket)$_2$(OTf)$_2$].

Compound	**[Mo(^{Me}diket)$_2$(OTf)$_2$]**	**[Mo(^{tBu}diket)$_2$(OTf)$_2$]**	**[Mo(^{Ph}diket)$_2$(OTf)$_2$]**
Empirical formula	$C_{12}H_{14}F_6MoO_{10}S_2$	$C_{24}H_{38}F_6MoO_{10}S_2$	$C_{32}H_{22}F_6MoO_{10}S_2$
Formula weight	592.29	760.60	877.61
Temperature [K]	100.0	100.0	100.01(10)
Crystal system	monoclinic	monoclinic	triclinic
Space group	Cc	C2/c	P-1
a [Å]	8.2697(3)	10.835(3)	13.7857(4)
b [Å]	12.9257(5)	16.573(4)	17.3581(5)
c [Å]	19.5683(6)	18.382(5)	23.1607(9)
α [°]	90	90	84.847(3)

β [°]	99.611(3)	96.369(4)	78.243(3)
γ [°]	90	90	88.840(2)
Volume [Å^3]	2062.33(13)	3280.5(14)	5404.0(3)
Z	4	4	6
ρ_{calc}g [cm^3]	1.908	1.540	1.618
μ [mm^{-1}]	8.079	0.609	4.862
F(000)	1176.0	1560.0	2658.0
Crystal size [mm^3]	0.04 × 0.03 × 0.01	0.615 × 0.366 × 0.194	0.144 × 0.056 × 0.037
Radiation	Cu Kα (λ = 1.54184)	MoKα (λ = 0.71073)	Cu Kα (λ = 1.54184)
2Θ range for data collection [°]	9.168 to 159.86	4.46 to 52.774	5.112 to 136.494
Index ranges	-10 ≤ h ≤ 10, -15 ≤ k ≤ 16, -25 ≤ l ≤ 22	-13 ≤ h ≤ 9, -13 ≤ k ≤ 20, -22 ≤ l ≤ 22	-16 ≤ h ≤ 16, -16 ≤ k ≤ 20, -27 ≤ l ≤ 27
Reflections collected	7189	5413	86791
Independent reflections	2598 [R_{int} = 0.0363, R_{sigma} = 0.0412]	3255 [R_{int} = 0.0300, R_{sigma} = 0.0542]	19763 [R_{int} = 0.0876, R_{sigma} = 0.0630]
Data/restraints/ parameters	2598/2/284	3255/0/201	19763/54/1472
Goodness-of-fit on F^2	1.066	1.084	1.043
Final R indexes [I>=2σ (I)]	R_1 = 0.0382, wR_2 = 0.0990	R_1 = 0.0523, wR_2 = 0.1342	R_1 = 0.0594, wR_2 = 0.1487
Final R indexes [all data]	R_1 = 0.0396, wR_2 = 0.0999	R_1 = 0.0635, wR_2 = 0.1455	R_1 = 0.0874, wR_2 = 0.1636
Largest diff. peak/hole [e Å^{-3}]	0.76/-1.12	1.38/-0.65	1.62/-1.55

Table S6: Refinement details of crystal structures of triflate complexes [Mo(O)($^{t\text{Bu}}$diket)$_2$(OTf)] and [Mo(N)($^{t\text{Bu}}$diket)$_2$(OTf)].

Compound	**[Mo(O)($^{t\text{Bu}}$diket)$_2$(OTf)]**	**[Mo(N)($^{t\text{Bu}}$diket)$_2$(OTf)]**
Empirical formula	$C_{23}H_{38}F_3MoO_8S$	$C_{23}H_{38}F_3MoNO_7S$
Formula weight	627.53	625.54
Temperature [K]	100.0	100.0
Crystal system	orthorhombic	monoclinic
Space group	$Pca2_1$	$P2_1/c$
a [Å]	19.0456(2)	12.5385(7)
b [Å]	17.89060(10)	13.0927(7)
c [Å]	17.08060(10)	17.3859(10)
α [°]	90	90
β [°]	90	97.315(2)
γ [°]	90	90
Volume [Å^3]	5820.00(8)	2830.9(3)
Z	8	4

ρ_{calc}g [cm^3]	1.432	1.468
μ [mm^{-1}]	4.892	0.597
F(000)	2600.0	1296.0
Crystal size [mm^3]	0.162 × 0.096 × 0.056	0.311 × 0.252 × 0.226
Radiation	CuKα (λ = 1.54184)	MoKα (λ = 0.71073)
2Θ range for data collection [°]	4.94 to 160.316	4.518 to 61.064
Index ranges	-24 ≤ h ≤ 23, -21 ≤ k ≤ 22, -21 ≤ l ≤ 18	-17 ≤ h ≤ 17, -18 ≤ k ≤ 18, -24 ≤ l ≤ 24
Reflections collected	31035	64330
Independent reflections	10297 [R_{int} = 0.0388, R_{sigma} = 0.0413]	8625 [R_{int} = 0.0381, R_{sigma} = 0.0244]
Data/restraints/ parameters	10297/337/766	8625/0/337
Goodness-of-fit on F^2	1.070	1.055
Final R indexes [I>=2σ (I)]	R_1 = 0.0304, wR_2 = 0.0780	R_1 = 0.0228, wR_2 = 0.0521
Final R indexes [all data]	R_1 = 0.0314, wR_2 = 0.0785	R_1 = 0.0300, wR_2 = 0.0562
Largest diff. peak/hole [e Å^{-3}]	0.49/-0.59	0.46/-0.48

4.3 Metrics

Most important bond lengths and comparison to literature solid state structures. For diketonate chelating ligands with non-identical Mo-O bond lengths, the overall average is given. Literature values are displayed in gray.

The bending angle of the diketonate ligand bound to Mo (∡) was defined by the angle between the two planes spanned by i.) the Mo-center and the two coordinating oxygen atoms and ii.) by the central carbon of the diketonate ligand and the two coordinating oxygen atoms, respectively.

Table S7: Selected bond lengths and bending angles of in here reported complexes as well as selected literature exemples for comparison (in *gray*).

Compound	$d_{Mo\text{-}O(diket)}$ **[Å]**	$d_{Mo\text{-}Cl}$ **[Å]**	$d_{Mo\text{-}O(Tf)}$ **[Å]**	$d_{Mo=O}$ **[Å]**	$d_{Mo\equiv N}$**[Å]**	∡ **[°]**
[Mo(^{Me}diket)$_2$Cl$_2$]	2.0095(7)	2.3763(7)				21.4
[Mo(^{tBu}diket)$_2$Cl$_2$]	2.004(13)	2.375(2)				25.4
[Mo(^{Ph}diket)$_2$Cl$_2$(py)]	2.065(10)	2.405(5)				25.8 ± 1.6
[Mo(^{Me}diket)$_2$(OTf)$_2$]	1.97(2)		2.091(6)			12.8
[Mo(^{tBu}diket)$_2$(OTf)$_2$]	1.97(2)		2.074(3)			18.9
[Mo(^{Ph}diket)$_2$(OTf)$_2$]	1.97(2)		2.078(16)			23 ± 4
[Mo(O)(^{tBu}diket)$_2$(OTf)]	1.99(5)		2.347(4)	1.725(11)		12.4
[Mo(N)(^{tBu}diket)$_2$(OTf)]	2.00(2)		2.3941(10)		1.6456(11)	21.4
[Mo(^{Me}diket)$_3$][8, 9]	2.07					4.2 ± 1.1
[{Mo(O)(^{tBu}diket)$_2$}$_2$-μ-O][10]	2.09			1.679		7.7 ± 0.9
[Mo(O)$_2$(^{Me}diket)$_2$][11]	2.09			1.701		22.1
[Cp$_2$Mo(H)OTf][12]			2.186			
[Mo(S)(OTf)(dmpe)$_2$]OTf[13]			2.291(2)			
[Mo(NMe)(OTf)$_2$(PC≡CP)][14]			2.219			

We have observed that the Mo-OTf bond lengths ($d_{Mo\text{-}OTf}$ = 2.07 Å for [Mo^{IV}(^{tBu}diket)$_2$(OTf)$_2$]) are rather short when compared to previously reported solid state structures of Mo(IV)-triflate complexes, all

of them displaying Mo-OTf distances in the range of 2.20 ± 0.30 Å.[12-14] This comparatively stronger triflate anion binding is also in line with solution ^{19}F NMR spectra.

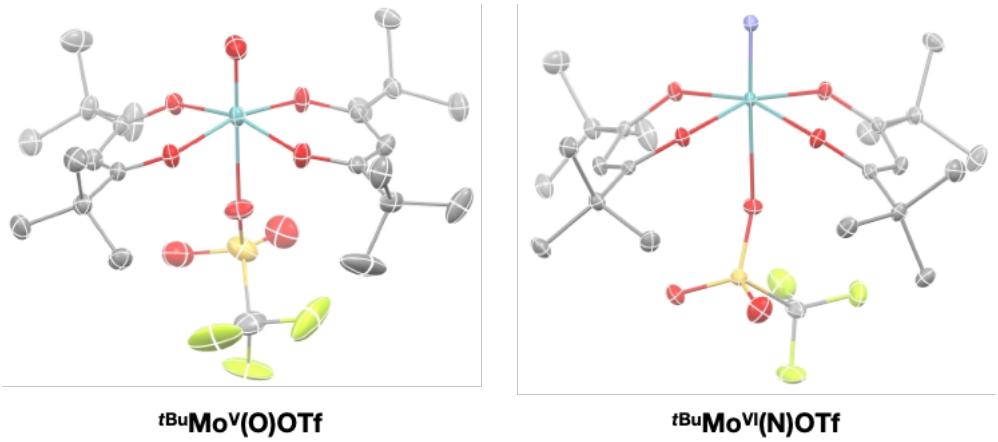

^{tBu}Mo^{V}(O)OTf ^{tBu}Mo^{VI}(N)OTf

Figure S19: Crystal structures of [Mo^{V}(O)(^{tBu}diket)$_2$(OTf)] (**^{tBu}Mo^{V}(O)OTf**) and of [Mo^{VI}(N)(^{tBu}diket)$_2$(OTf)] (**^{tBu}Mo^{VI}(N)OTf**).

5. NMR Spectroscopy

Both the Mo(IV) dichloride and bistriflate complexes are paramagnetic compounds (high spin d^2), yet provide clean signals solution ^{1}H and ^{19}F (for bis-triflate complexes) NMR spectra. As an example, the ^{1}H and ^{19}F NMR spectra of [Mo(^{tBu}diket)$_2$Cl$_2$] and [Mo(^{tBu}diket)$_2$(OTf)$_2$] in benzene-d_6 are displayed in Figure S16 and Figure S17. At the difference with the single crystal structures presented in the main text (see also Section S4), both *cis*- and *trans*-isomers are observed in solution for all the complexes synthetized, independently of the anionic monodentate ligand (Cl^- *or* TfO^-) present. Nevertheless, the ratio between the two isomers appeared to be both dependent of the anion and the solvent used to measure the spectra.

We could assign the sets of signals for both stereo-isomers based on the relative integration of the methine C*H*- and ^{t}Bu CH_3 signals (1:18 for *trans* and 1:9:9 for *cis*), enabling the determination of the relative ratio summarized in Table 1 in the main text. A significant influence of the polarity of the media on the *cis:trans* ratio can be noticed, more polar solvents favoring the *cis* isomer. The behavior at different temperatures was studied by variable temperature (VT) NMR (see Section S5.2). While for [Mo(^{tBu}diket)$_2$Cl$_2$] the ratio is nearly independent on temperature, ^{1}H NMR spectra of the corresponding bistriflate complex showed substantial changes, the *cis* isomer being more favored at decreased temperature, in agreement with the single crystal data.

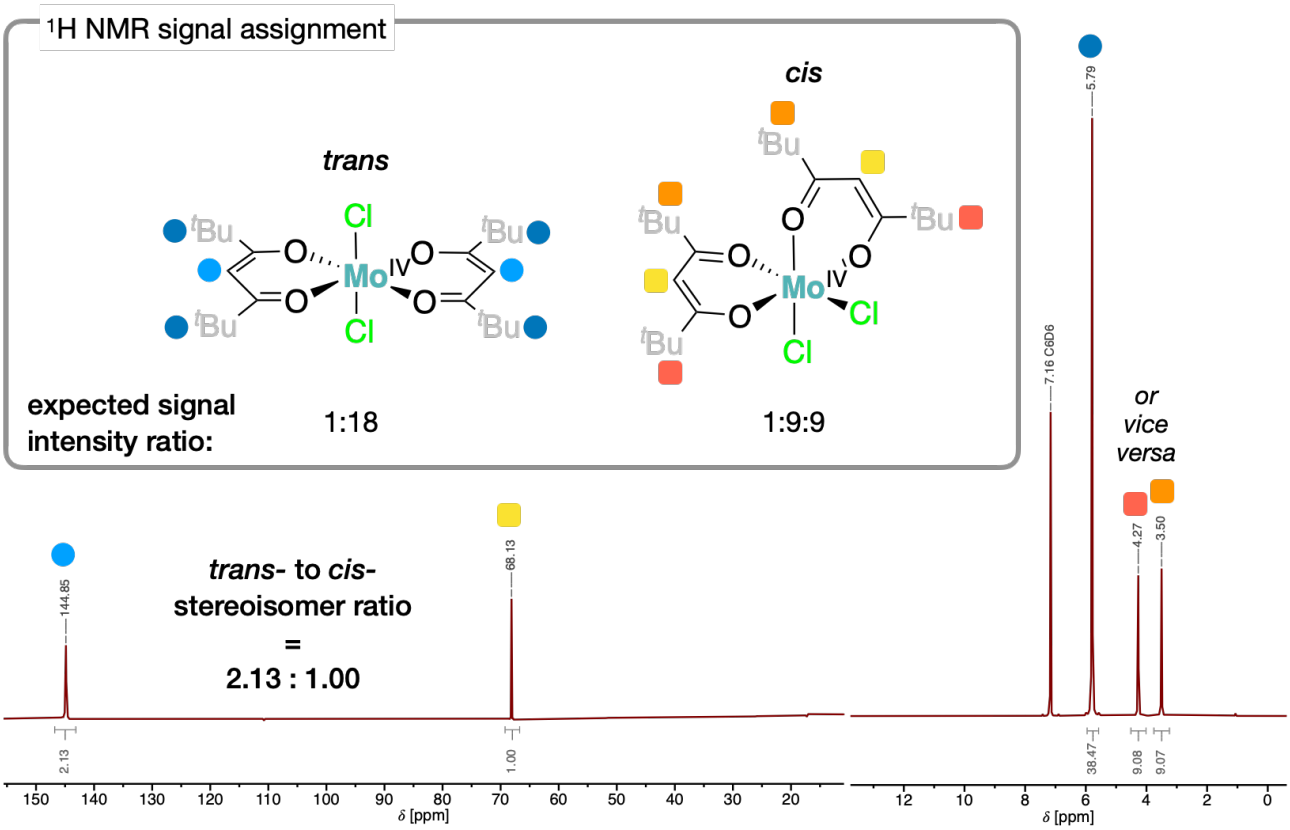

Figure S20: ^{1}H NMR spectrum of [Mo($^{t\mathrm{Bu}}$diket)$_2$Cl$_2$] in benzene-d_6 with signal assignments to protons of the corresponding stereoisomers.

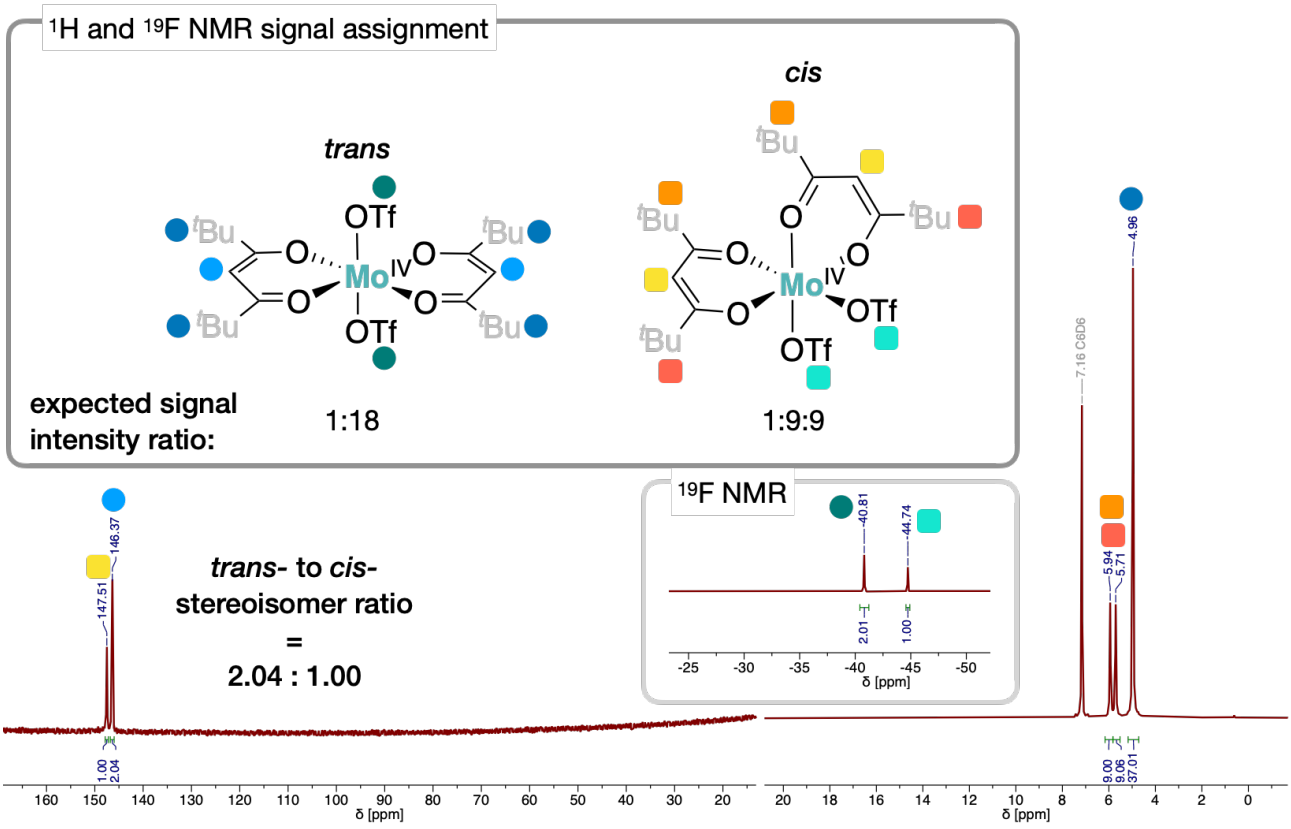

Figure S21: ^{1}H and ^{19}F NMR spectra of [Mo($^{t\mathrm{Bu}}$diket)$_2$Cl$_2$] in benzene-d_6 with signal assignments to protons and fluorine nuclei of the corresponding stereoisomers.

5.1 NMR Spectra of Isolated Metal Complexes

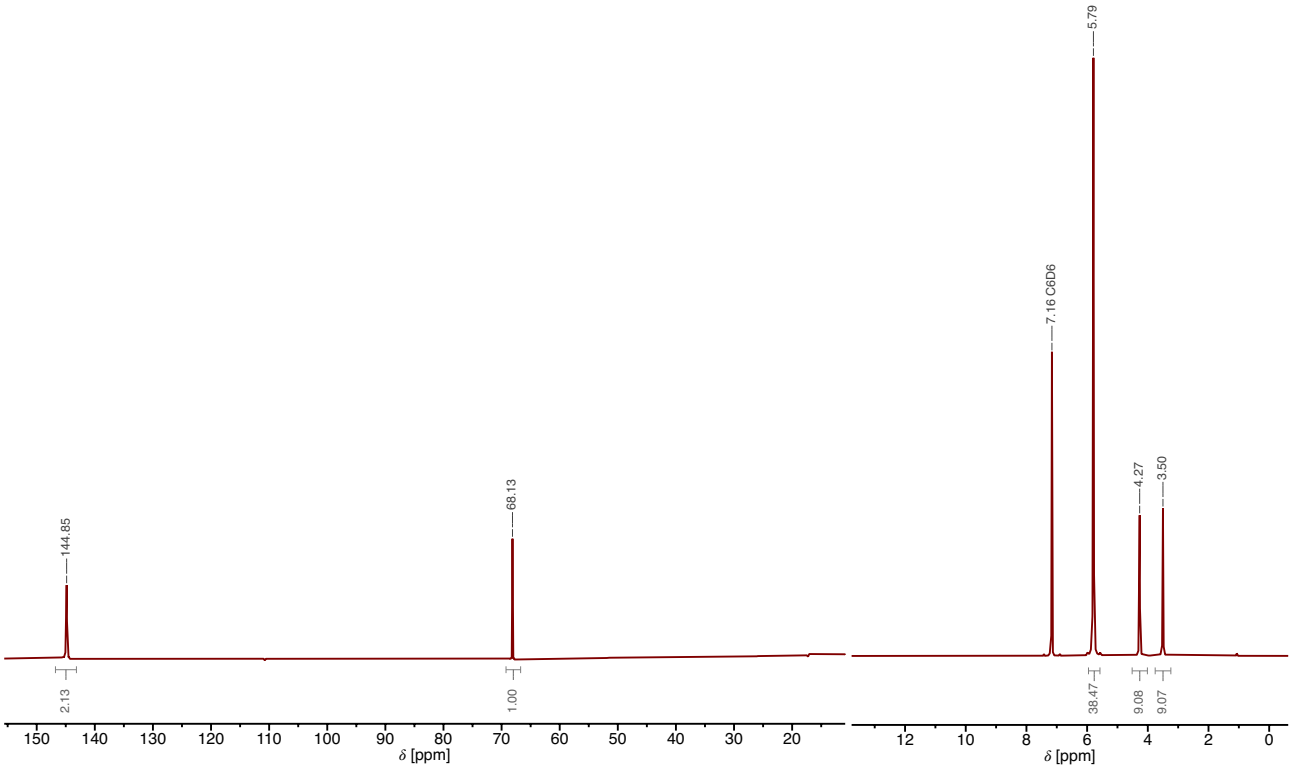

Figure S22: ^{1}H NMR spectrum of [Mo($^{t\text{Bu}}$diket)$_2$Cl$_2$] in benzene-d_6.

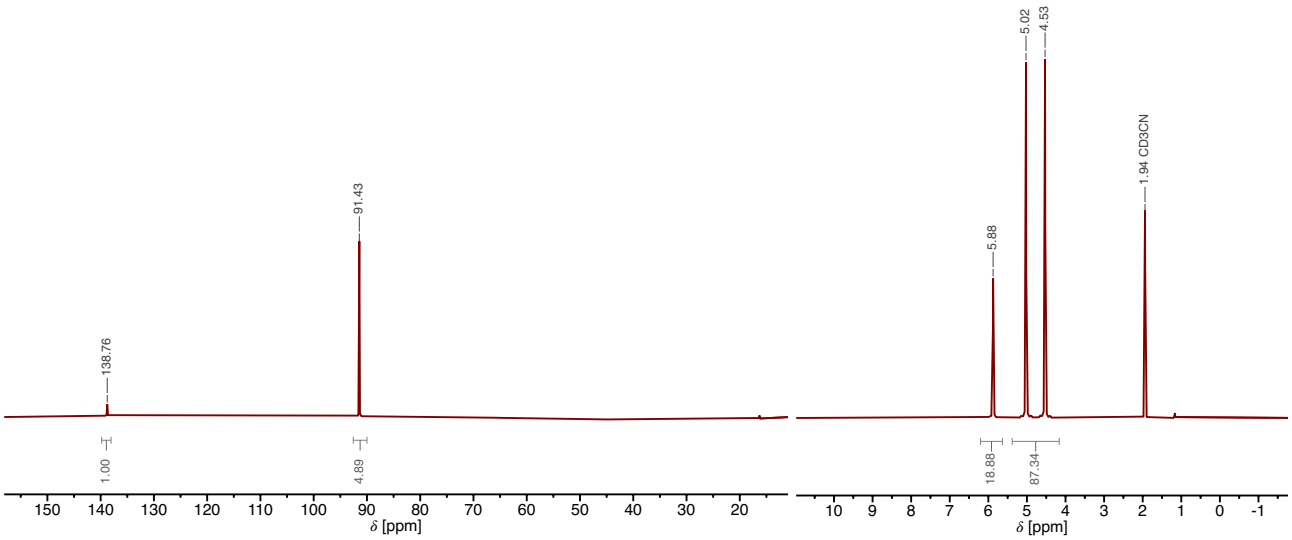

Figure S23: ^{1}H NMR spectrum of [Mo($^{t\text{Bu}}$diket)$_2$Cl$_2$] in MeCN-d_3.

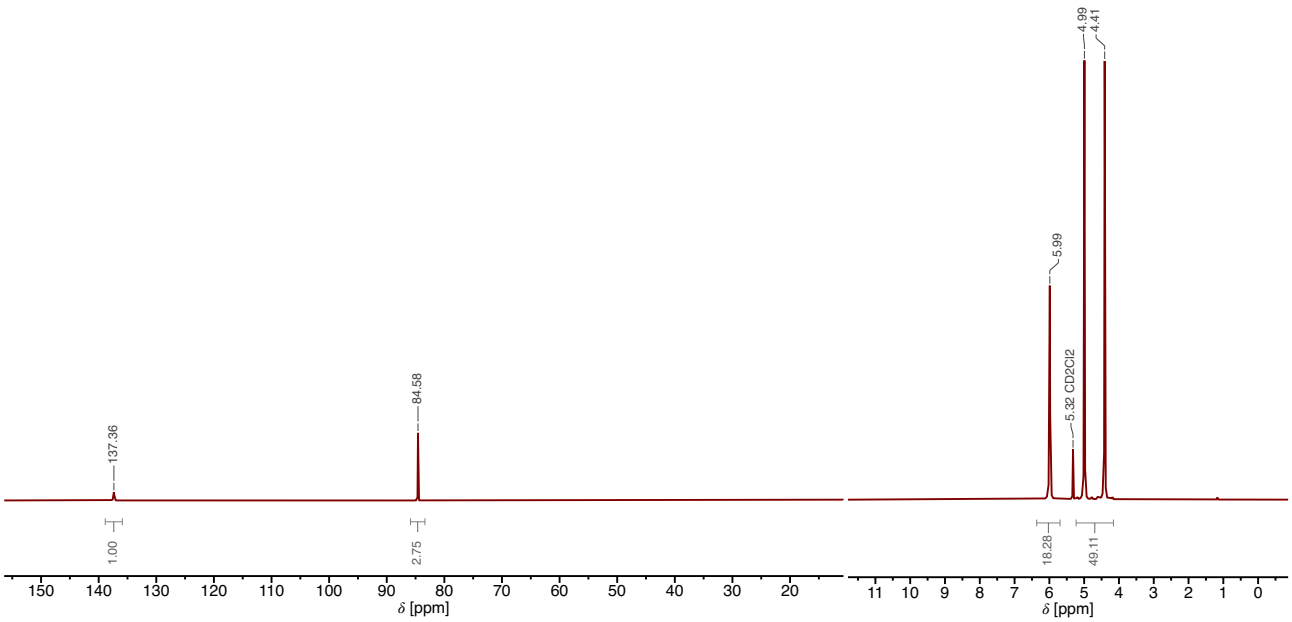

Figure S24: ^{1}H NMR spectrum of [Mo($^{t\text{Bu}}$diket)$_2$Cl$_2$] in CD_2Cl_2.

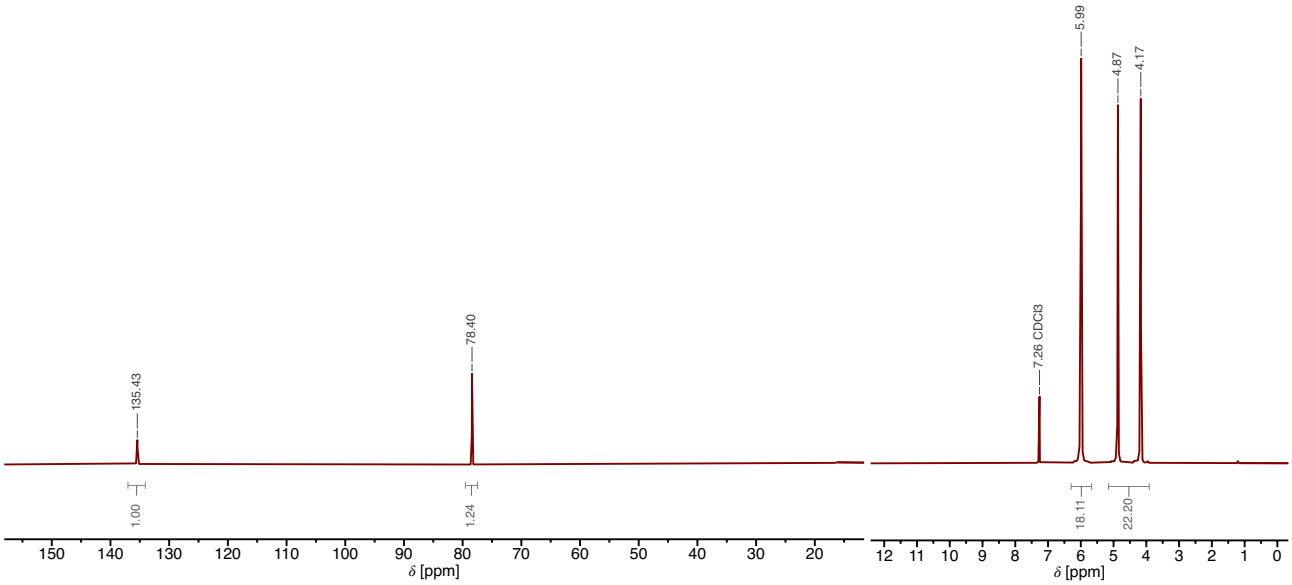

Figure S25: ^{1}H NMR spectrum of [Mo($^{t\text{Bu}}$diket)$_2$Cl$_2$] in $CDCl_3$.

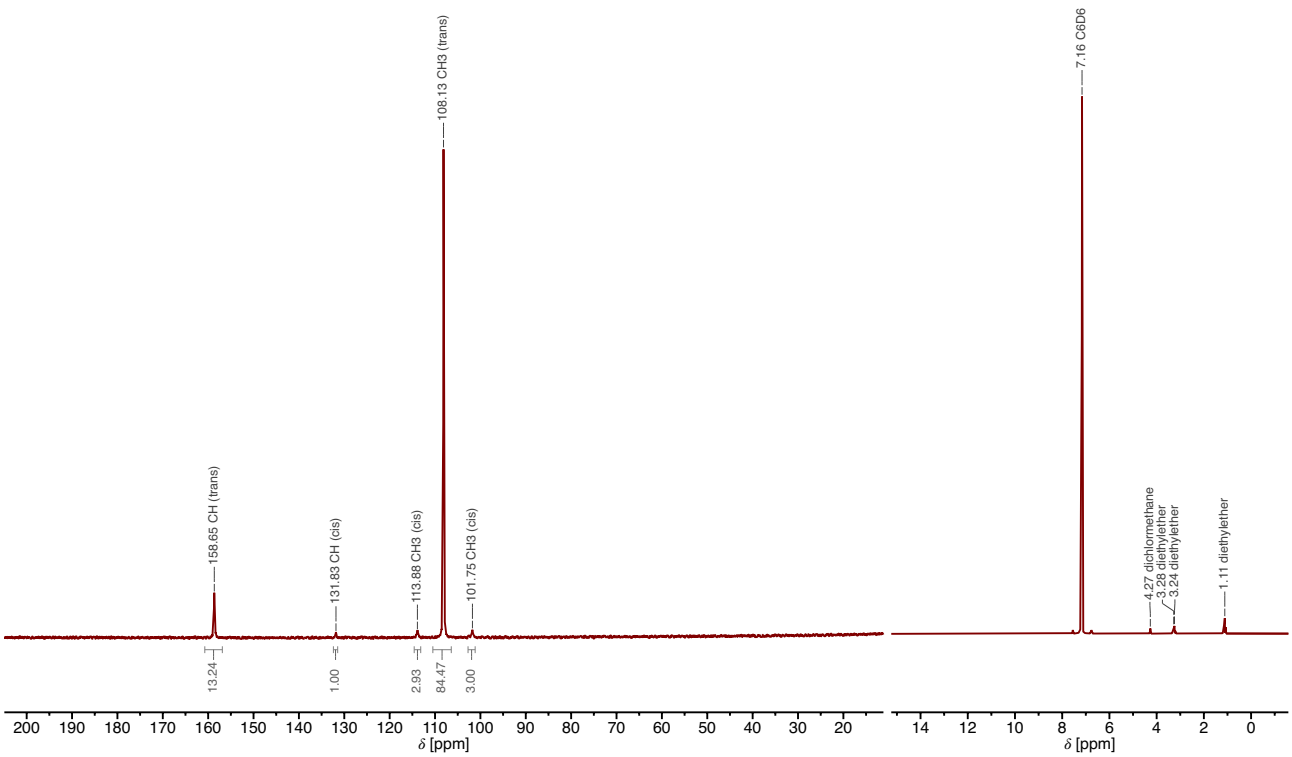

Figure S26: ^{1}H NMR spectrum of [Mo(^{Me}diket)$_2$(OTf)$_2$] in benzene-d_6.

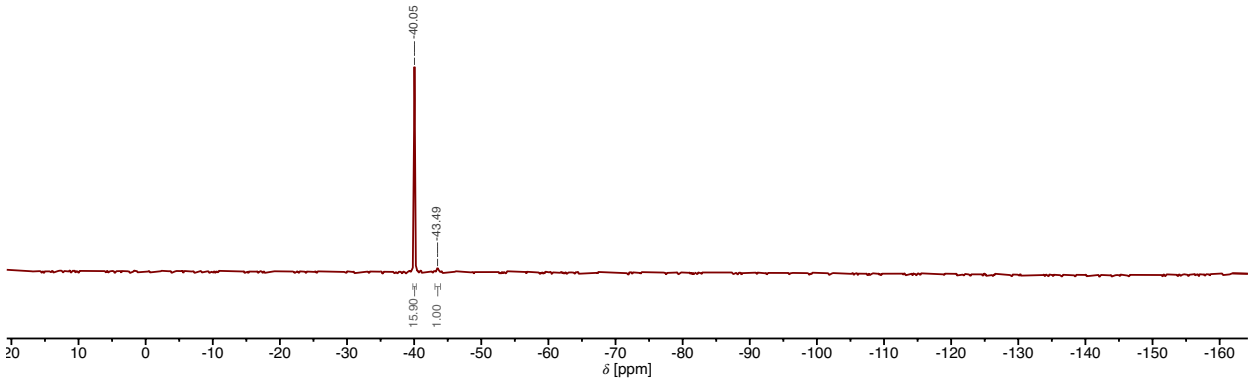

Figure S27: ^{19}F NMR spectrum of [Mo(^{Me}diket)$_2$(OTf)$_2$] in benzene-d_6.

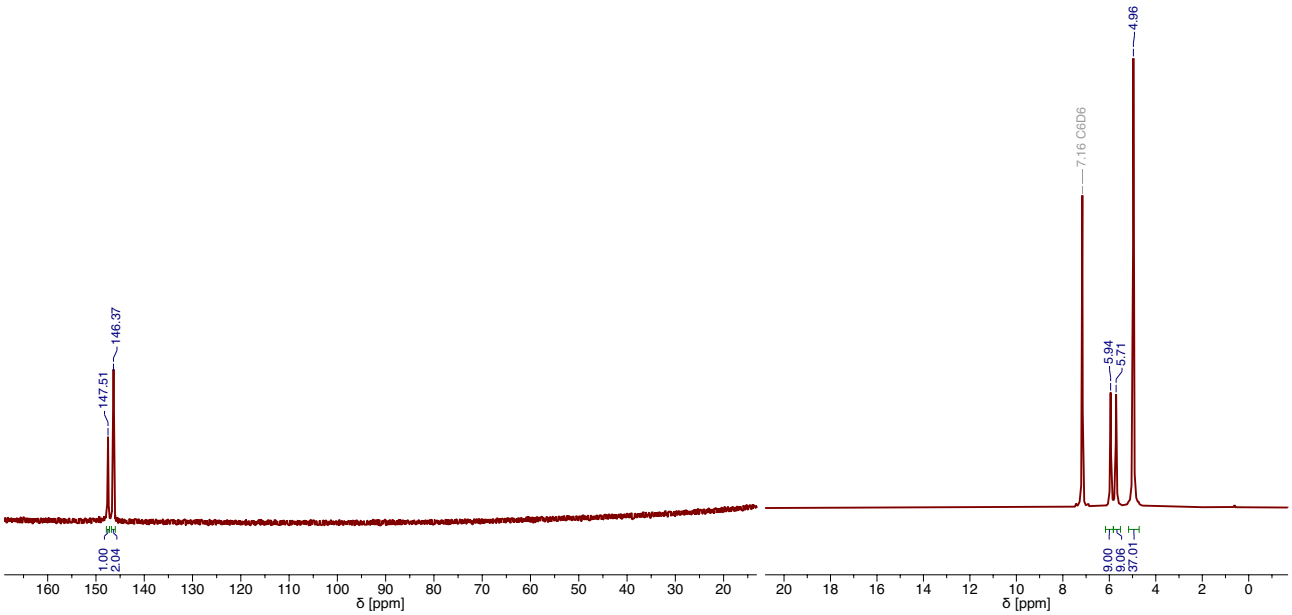

Figure S28: ^{1}H NMR spectrum of [Mo(^{tBu}diket)$_2$(OTf)$_2$] in benzene-d_6.

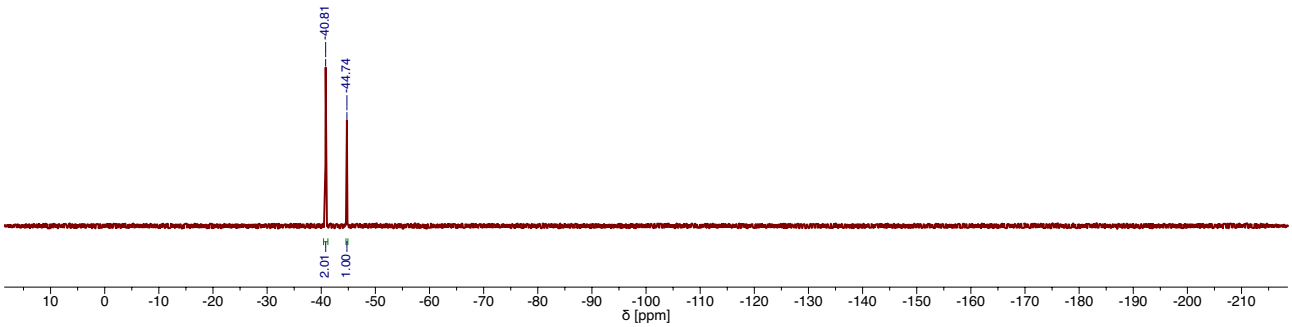

Figure S29: ^{19}F NMR spectrum of [Mo($^{t\text{Bu}}$diket)$_2$(OTf)$_2$] in benzene-d_6.

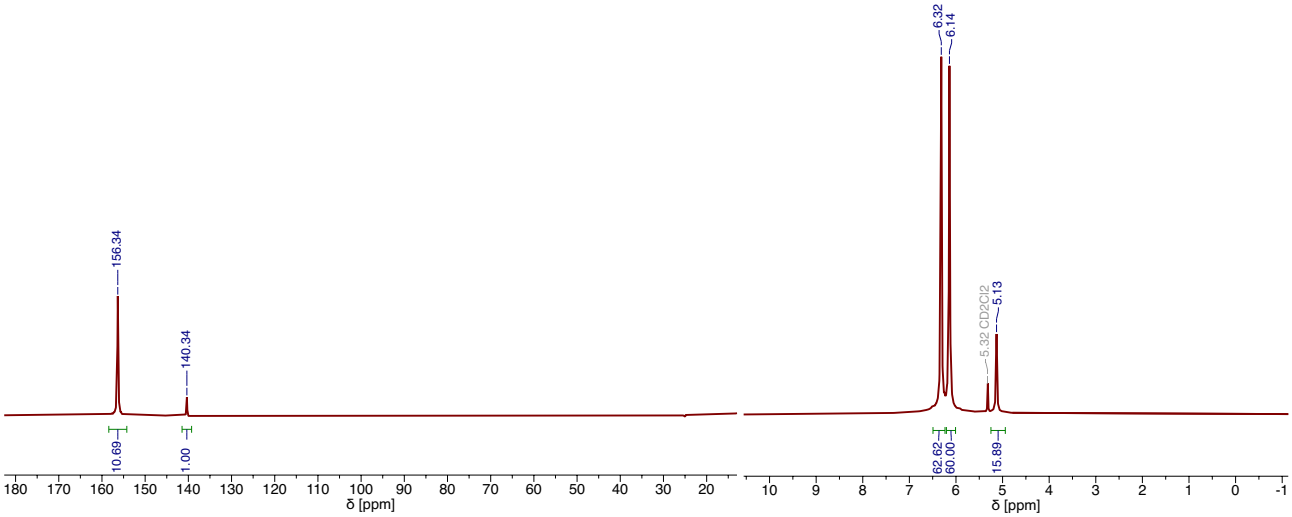

Figure S30: ^{1}H NMR spectrum of [Mo($^{t\text{Bu}}$diket)$_2$(OTf)$_2$] in CD_2Cl_2.

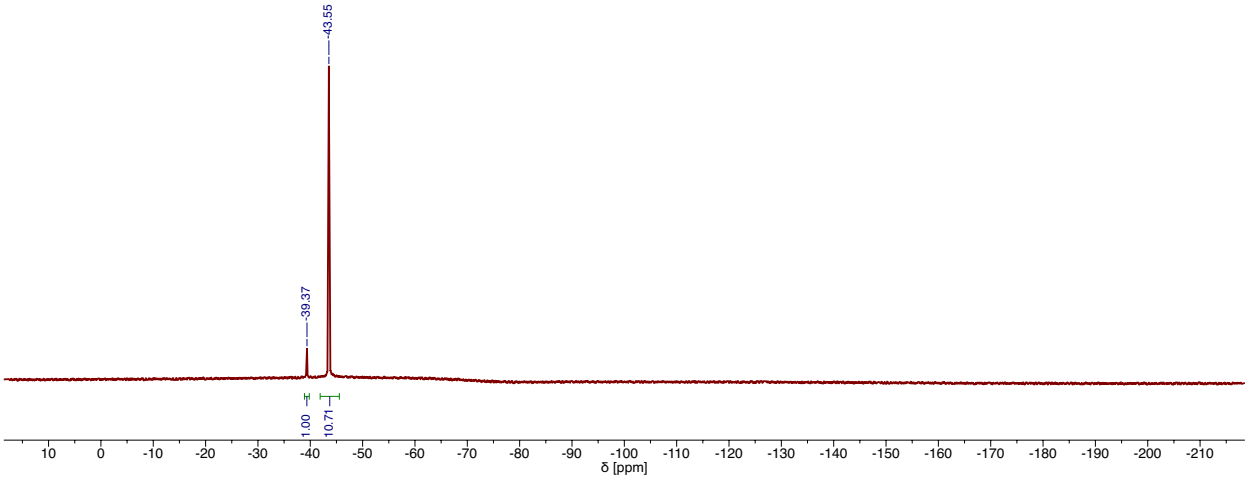

Figure S31: ^{19}F NMR spectrum of [Mo($^{t\text{Bu}}$diket)$_2$(OTf)$_2$] in CD_2Cl_2.

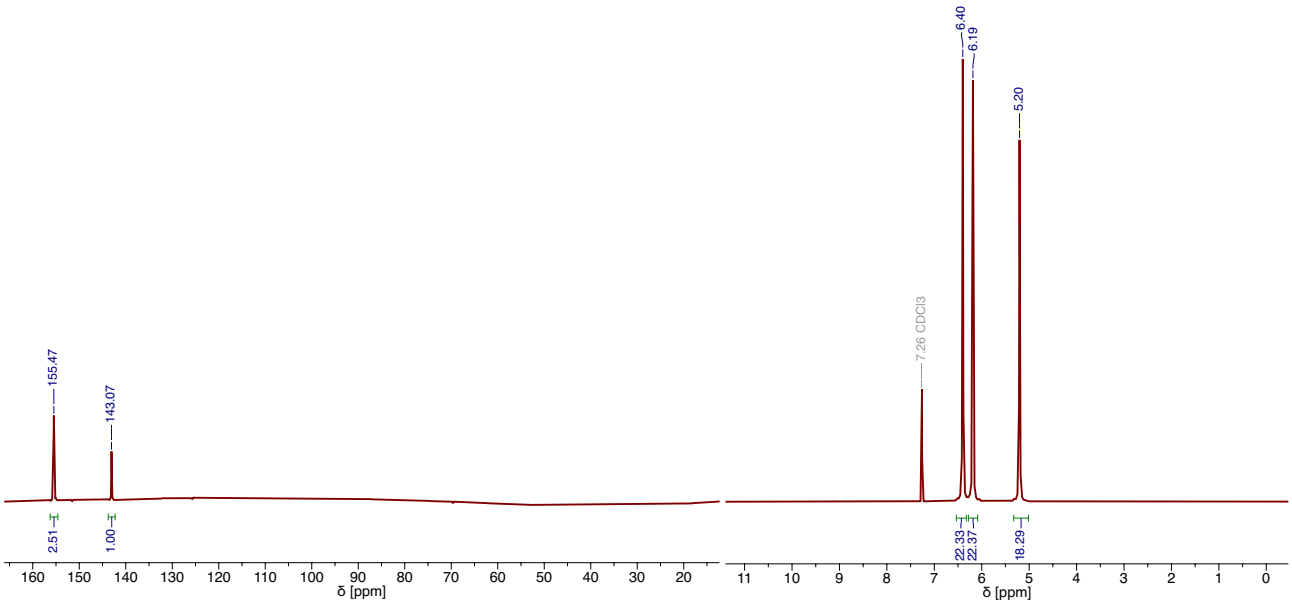

Figure S32: ^{1}H NMR spectrum of [Mo($^{t\text{Bu}}$diket)$_2$(OTf)$_2$] in $CDCl_3$.

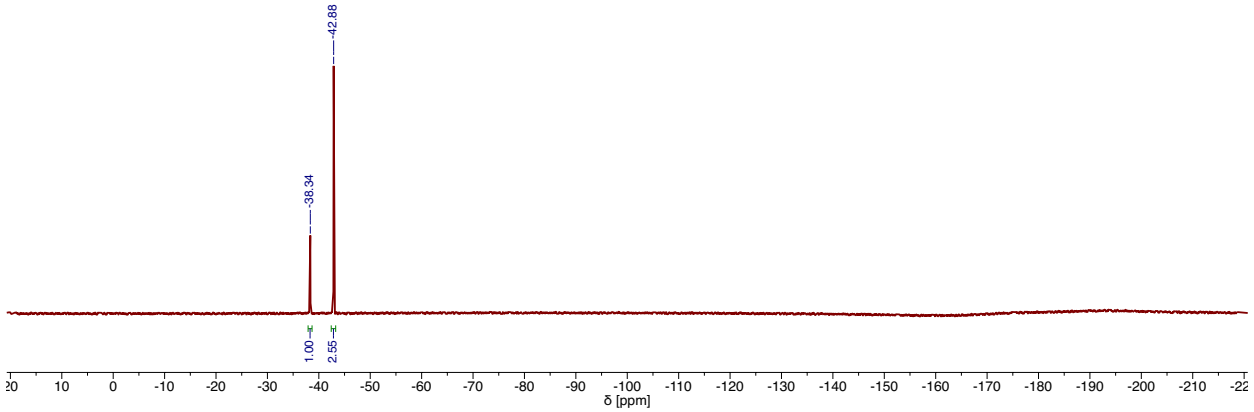

Figure S33: ^{19}F NMR spectrum of [Mo($^{t\text{Bu}}$diket)$_2$(OTf)$_2$] in $CDCl_3$.

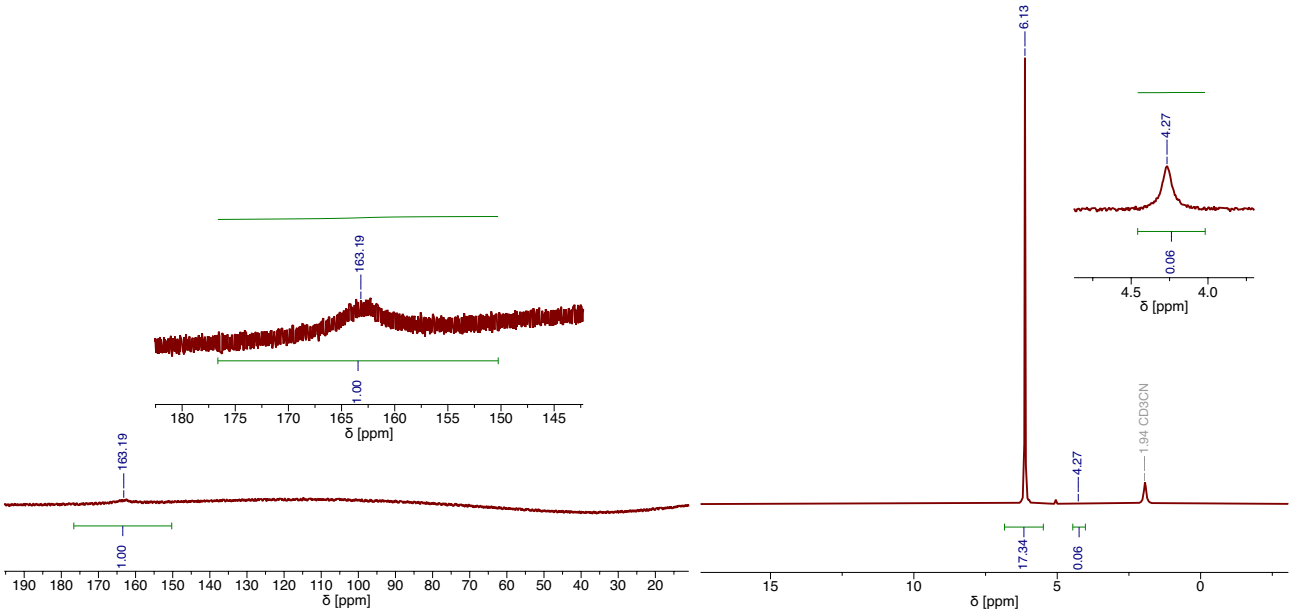

Figure S34: ^{1}H NMR spectrum of [Mo($^{t\text{Bu}}$diket)$_2$(OTf)$_2$] in MeCN-d_3.

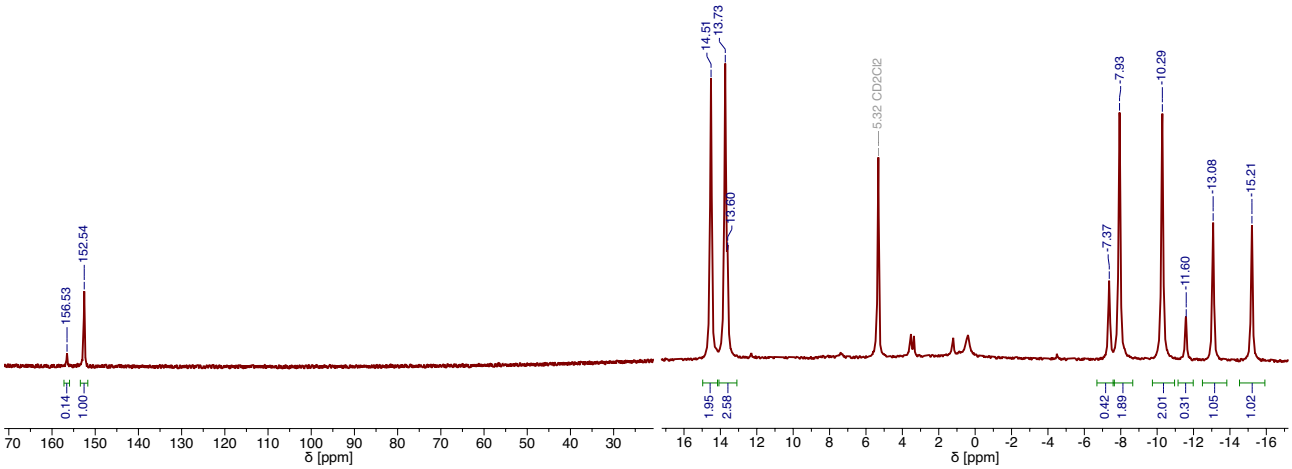

Figure S35: ^{1}H NMR spectrum of [Mo(^{Ph}diket)$_2$(OTf)$_2$] in CD_2Cl_2.

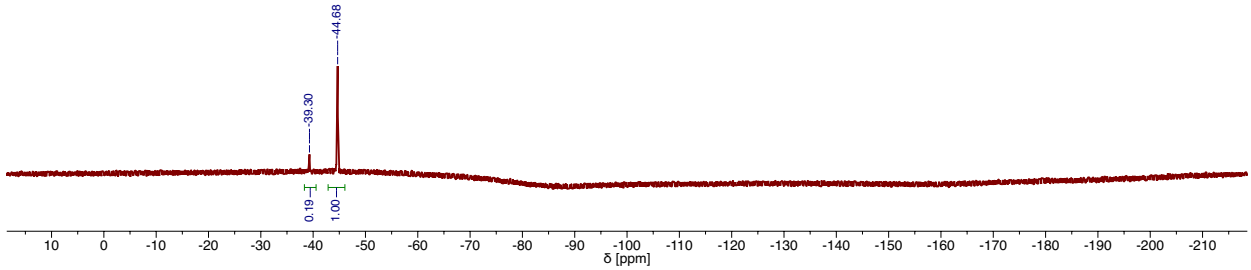

Figure S36: ^{19}F NMR spectrum of [Mo(^{Ph}diket)$_2$(OTf)$_2$] in CD_2Cl_2.

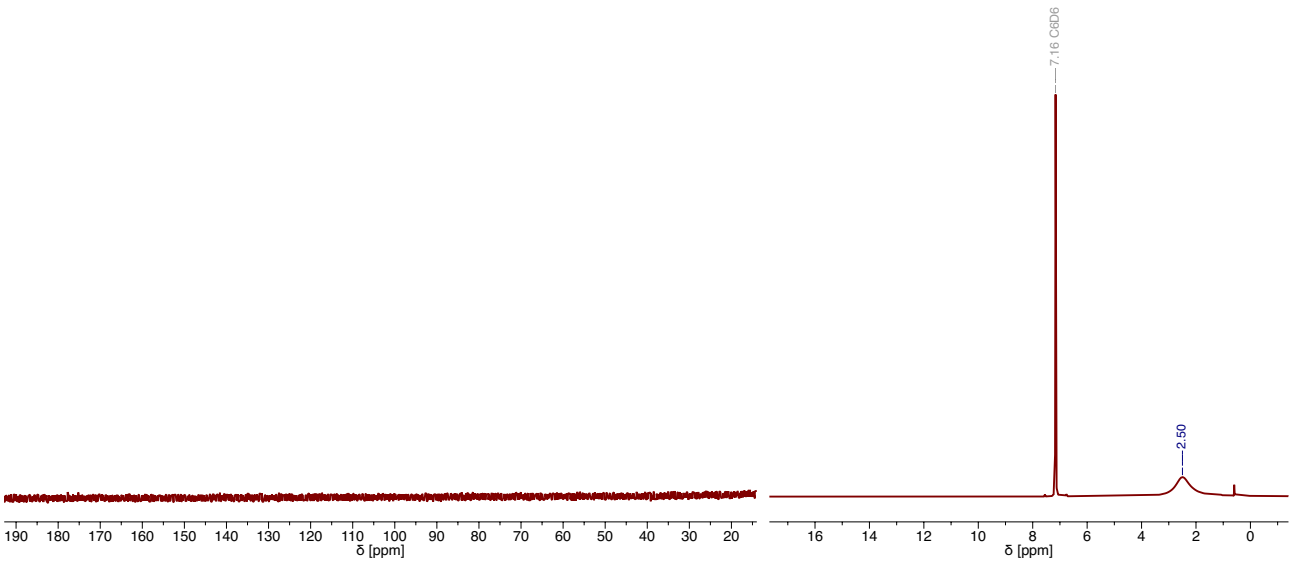

Figure S37: ^{1}H NMR spectrum of [Mo(O)(^{tBu}diket)$_2$(OTf)] in benzene-d_6.

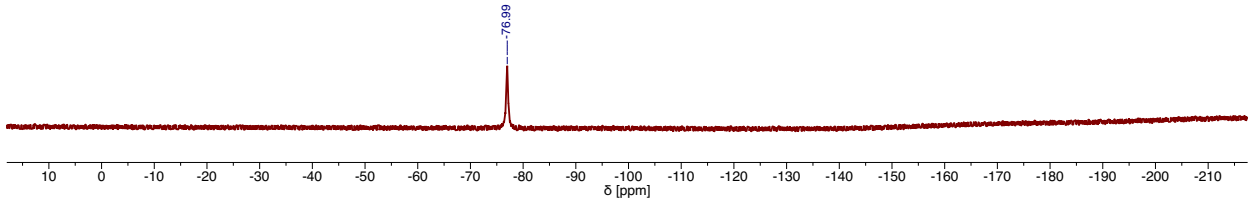

Figure S38: ^{19}F NMR spectrum of [Mo(O)(^{tBu}diket)$_2$(OTf)] in benzene-d_6.

5.1 VT NMR Studies of [Mo($^{t\text{Bu}}$diket)$_2$Cl$_2$] and [Mo($^{t\text{Bu}}$diket)$_2$(OTf)$_2$]

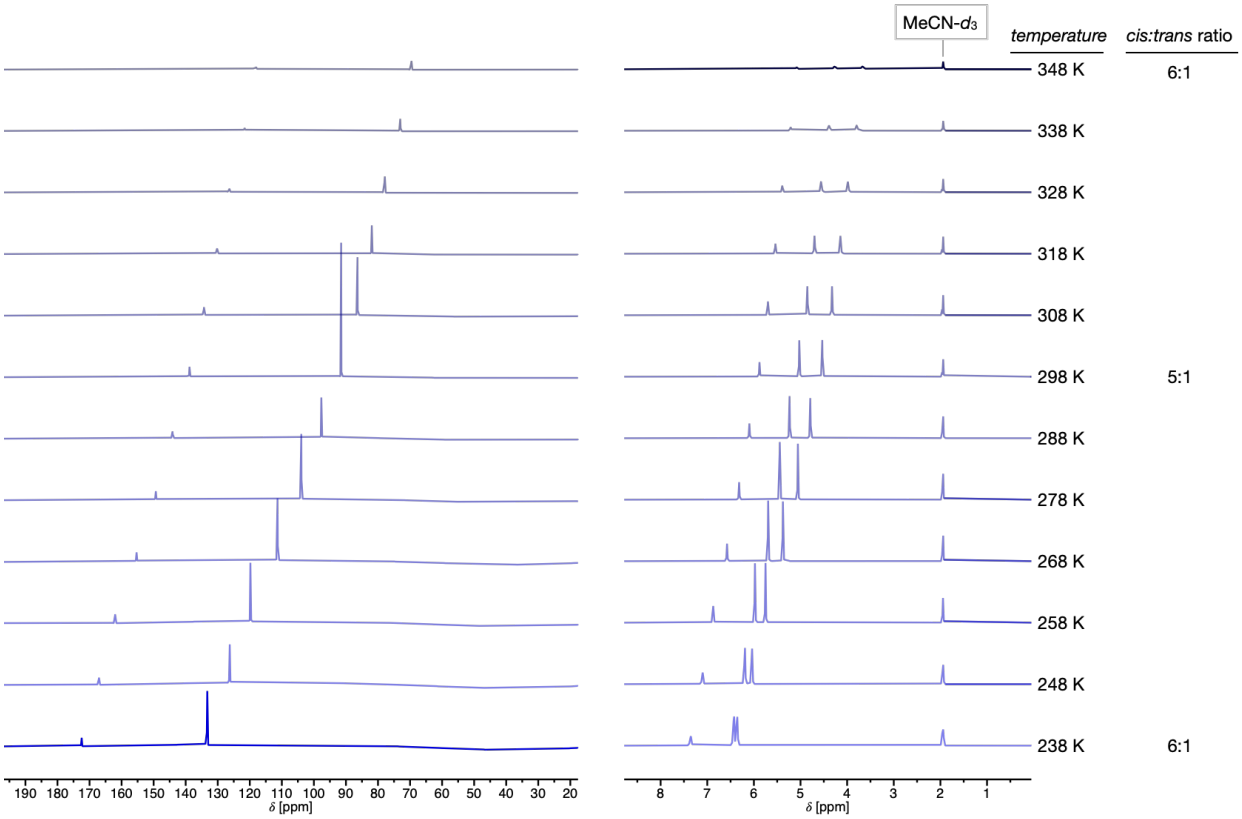

Figure S39: VT ^{1}H NMR spectra of [Mo($^{t\text{Bu}}$diket)$_2$Cl$_2$] in MeCN-d_3.

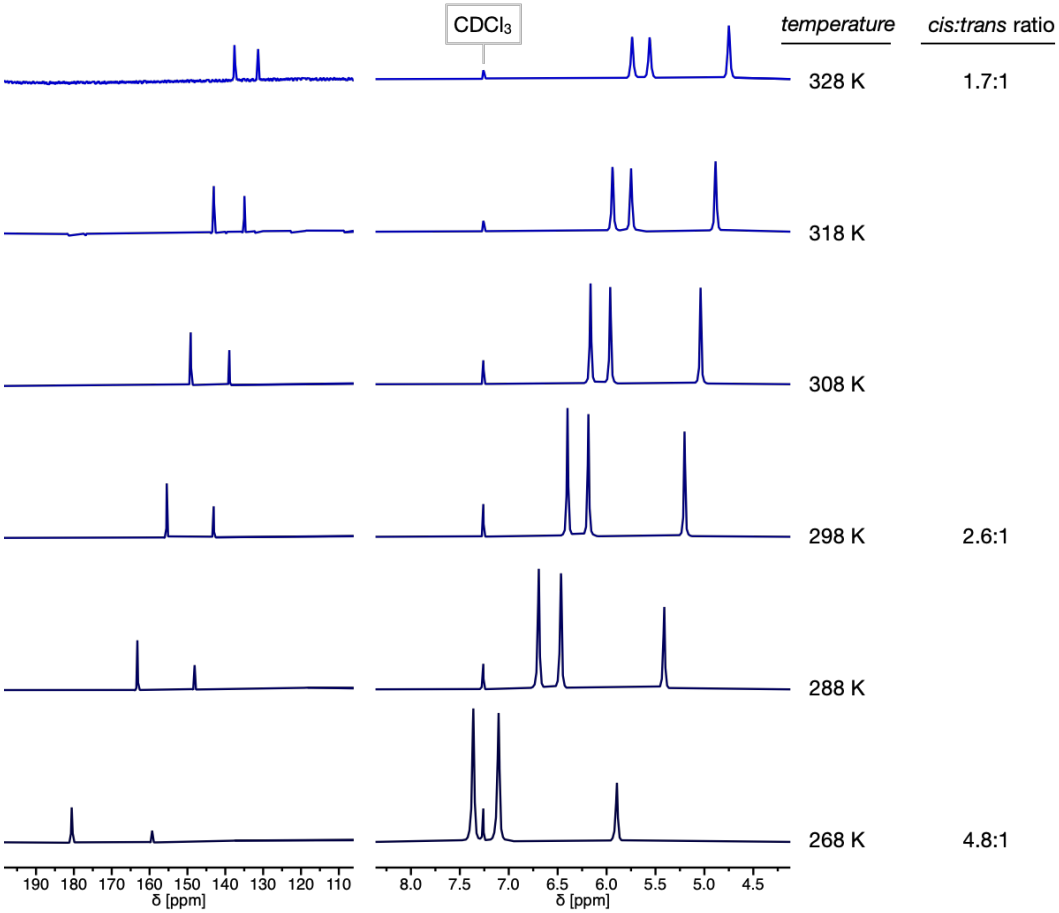

Figure S40: VT ^{1}H NMR spectra of [Mo($^{t\text{Bu}}$diket)$_2$(OTf)$_2$] in $CDCl_3$.

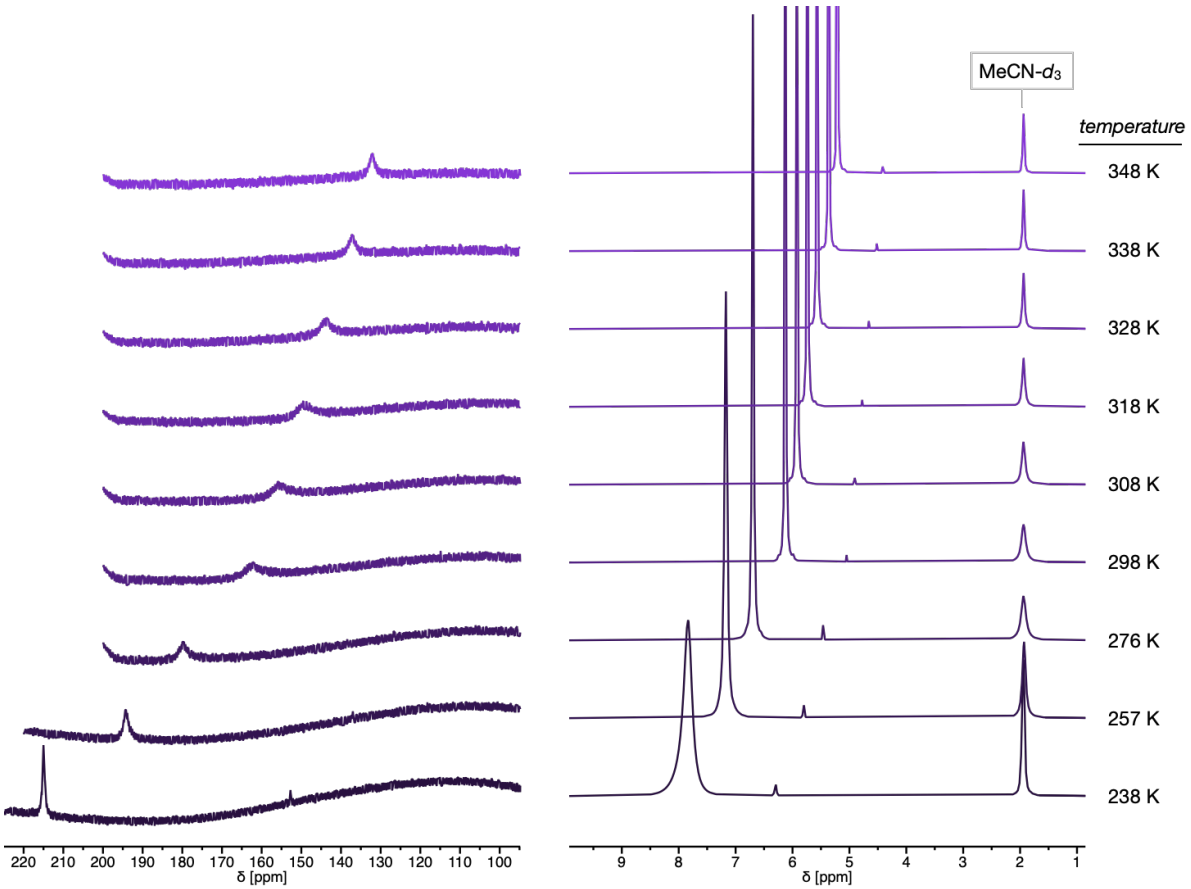

Figure S41: VT ^{1}H NMR spectra of [Mo($^{t\text{Bu}}$diket)$_2$(OTf)$_2$] in MeCN-d_3.

6. UV-Vis Spectra

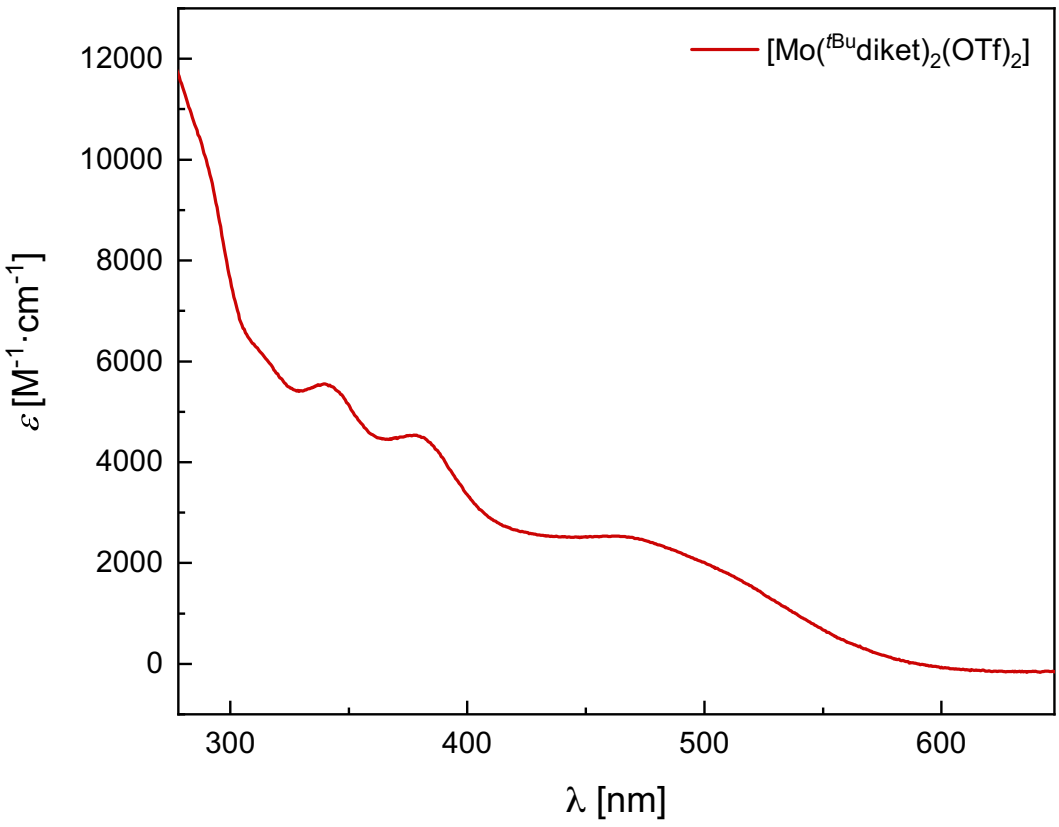

Figure S42: UV-Vis spectrum of [Mo^{IV}($^{t\text{Bu}}$diket)$_2$(OTf)$_2$] in CH_2Cl_2 (d = 2 mm).

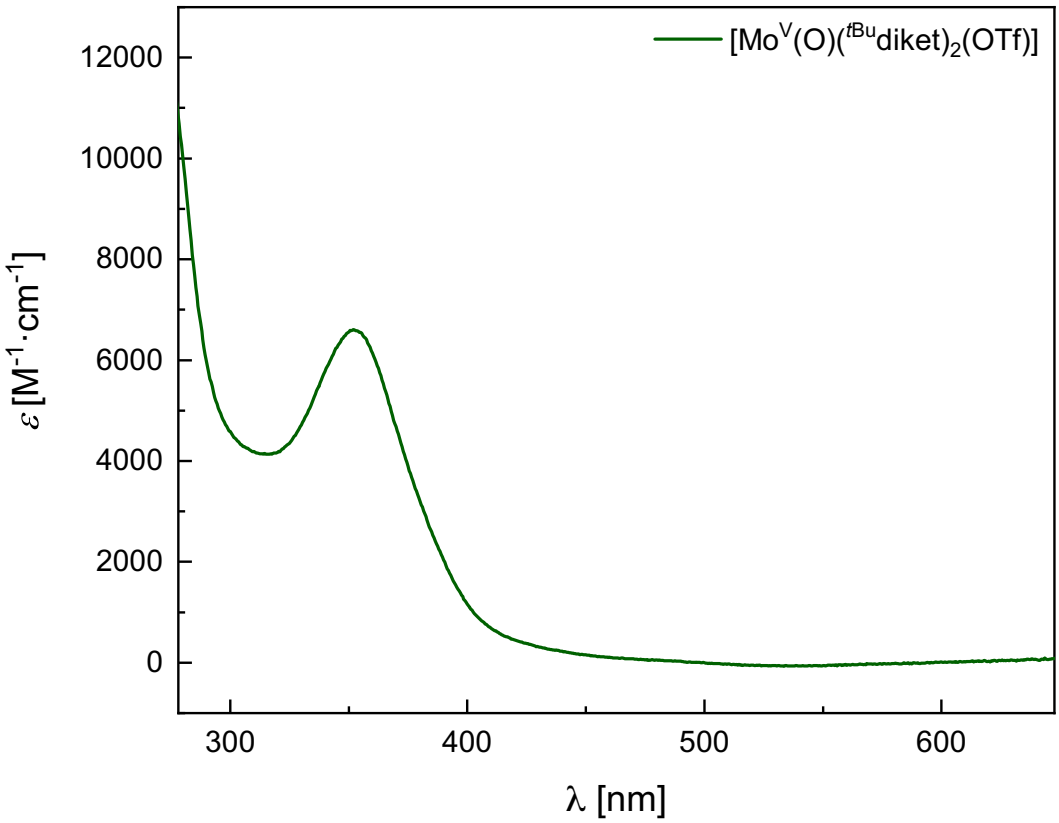

Figure S43: UV-Vis spectrum of [Mo^{V}(O)($^{t\text{Bu}}$diket)$_2$(OTf)] in CH_2Cl_2 (*d* = 2 mm).

7. Computational Details

DFT calculations were performed using the Gaussian 09 program.[15] The UPBE1PBE functional, in combination with SDD (for Mo) and Def2VP (for all lighter atoms) basis sets, was employed.

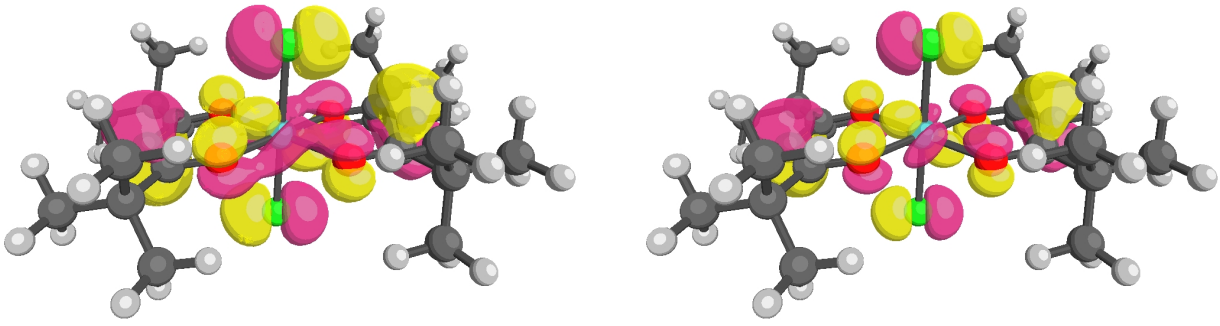

Figure S44: Computed alpha molecular orbital 123 (HOMO-3) of [Mo($^{t\text{Bu}}$diket)$_2$Cl$_2$]. Iso value = 0.08 (*left*) and 0.11 (*right*).

Table S8: Coordinates of geometry optimized structure of [Mo($^{t\text{Bu}}$diket)$_2$Cl$_2$].

Mo	0	0	0	**O**	-0.03533	-0.99273	-1.7718
Cl	-1.91743	-1.18994	0.72739	**C**	0.79842	2.93237	3.71181
Cl	1.91743	1.18994	-0.72739	**C**	0.42987	1.15256	5.43713
O	1.18431	-1.33296	0.97316	**C**	2.5056	-2.95118	4.015
O	0.03533	0.99273	1.7718	**C**	1.41697	-3.95391	1.9947
O	-1.18431	1.33296	-0.97316	**C**	3.56319	-2.6679	1.76207

C	-1.46937	1.88388	3.97786
C	1.04513	-0.58477	3.20443
C	2.23171	-2.76297	2.52418
C	1.4381	-1.49588	2.21246
C	0.04572	1.63263	4.03894
C	0.3845	0.625	2.9423
C	-0.79842	-2.93237	-3.71181
C	-0.42987	-1.15256	-5.43713
C	-2.5056	2.95118	-4.015
C	-1.41697	3.95391	-1.9947
C	-3.56319	2.6679	-1.76207
C	1.46937	-1.88388	-3.97786
C	-1.04513	0.58477	-3.20443
C	-2.23171	2.76297	-2.52418
C	-1.4381	1.49588	-2.21246
C	-0.04572	-1.63263	-4.03894
C	-0.3845	-0.625	-2.9423
H	1.88872	2.78312	3.75058
H	0.53356	3.71075	4.44409
H	0.53719	3.29223	2.70696
H	-0.08902	0.22067	5.7094
H	0.14419	1.91659	6.17591
H	1.51418	0.99088	5.53602
H	3.11001	-2.13064	4.43106
H	3.07043	-3.88348	4.1664
H	1.57561	-3.03166	4.59842
H	0.45193	-4.04211	2.51726
H	1.97889	-4.88773	2.15059
H	1.21328	-3.8415	0.92086
H	3.38912	-2.53296	0.68559
H	4.14367	-3.5914	1.91158
H	4.16933	-1.8213	2.12041
H	-1.76557	2.24435	2.98317
H	-1.75104	2.64162	4.72521
H	-2.03649	0.96438	4.18987
H	1.31599	-0.80359	4.2315
H	-1.88872	-2.78312	-3.75058
H	-0.53356	-3.71075	-4.44409
H	-0.53719	-3.29223	-2.70696
H	0.08902	-0.22067	-5.7094
H	-0.14419	-1.91659	-6.17591
H	-1.51418	-0.99088	-5.53602
H	-3.11001	2.13064	-4.43106
H	-3.07043	3.88348	-4.1664
H	-1.57561	3.03166	-4.59842
H	-0.45193	4.04211	-2.51726
H	-1.97889	4.88773	-2.15059
H	-1.21328	3.8415	-0.92086
H	-3.38912	2.53296	-0.68559
H	-4.14367	3.5914	-1.91158
H	-4.16933	1.8213	-2.12041
H	1.76557	-2.24435	-2.98317
H	1.75104	-2.64162	-4.72521
H	2.03649	-0.96438	-4.18987
H	-1.31599	0.80359	-4.2315

1. A. van den Bergen, K. S. Murray and B. O. West, *Aust. J. Chem.*, 1972, **25**.
2. C. L. Ricardo, X. Mo, J. A. McCubbin and D. G. Hall, *Chem.*, 2015, **21**, 4218-4223.
3. M. M. Naik, D. P. Kamat, S. G. Tilve and V. P. Kamat, *Tetrahedron*, 2014, **70**, 5221-5233.
4. K. Watanabe, T. Mino, T. Abe, T. Kogure and M. Sakamoto, *J. Org. Chem.*, 2014, **79**, 6695-6702.
5. O. V. Dolomanov, L. J. Bourhis, R. J. Gildea, J. A. K. Howard and H. Puschmann, *J. Appl. Crystal.*, 2009, **42**, 339-341.
6. G. M. Sheldrick, *Acta Cryst.*, 2015, **71**, 3-8.
7. G. M. Sheldrick, *Acta Cryst.*, 2008, **64**, 112-122.
8. A. Y. Ledneva, S. B. Artemkina, D. A. Piryazev and V. E. Fedorov, *J. Struct. Chem.*, 2015, **56**, 1021-1023.

9. C. L. Raston and A. H. White, *Aust. J. Chem.*, 1979, **32**.

10. A. Y. Ledneva, S. B. Artemkina, P. A. Stabnikov, L. V. Yanshole and V. E. Fedorov, *J. Struct. Chem.*, 2017, **58**, 758-762.

11. D. H. Johnston, C. King, A. Seitz and M. Sethi, *IUCrData*, 2021, **6**, x210778.

12. L. Y. Kuo, T. J. R. Weakley, K. Awana and C. Hsia, *Organometallics*, 2001, **20**, 4969-4972.

13. S. J. Smith, C. M. Whaley, T. B. Rauchfuss and S. R. Wilson, *Inorg. Chem.*, 2006, **45**, 679-687.

14. H. K. Wagner, H. Wadepohl and J. Ballmann, *Angew. Chem., Int. Ed. Engl.*, 2021, **60**, 25804-25808.

15. Gaussian 09, Revision A.02, G. W. T. J. Frisch, H. B. Schlegel, G. E. Scuseria, M. A. Robb, J. R. Cheeseman, G. Scalmani, V. Barone, G. A. Petersson, H. Nakatsuji, X. Li, M. Caricato, A. Marenich, J. Bloino, B. G. Janesko, R. Gomperts, B. Mennucci, H. P. Hratchian, J. V. Ortiz, A. F. Izmaylov, J. L. Sonnenberg, D. Williams-Young, F. Ding, F. Lipparini, F. Egidi, J. Goings, B. Peng, A. Petrone, T. Henderson, D. Ranasinghe, V. G. Zakrzewski, J. Gao, N. Rega, G. Zheng, W. Liang, M. Hada, M. Ehara, K. Toyota, R. Fukuda, J. Hasegawa, M. Ishida, T. Nakajima, Y. Honda, O. Kitao, H. Nakai, T. Vreven, K. Throssell, J. A. Montgomery, Jr., J. E. Peralta, F. Ogliaro, M. Bearpark, J. J. Heyd, E. Brothers, K. N. Kudin, V. N. Staroverov, T. Keith, R. Kobayashi, J. Normand, K. Raghavachari, A. Rendell, J. C. Burant, S. S. Iyengar, J. Tomasi, M. Cossi, J. M. Millam, M. Klene, C. Adamo, R. Cammi, J. W. Ochterski, R. L. Martin, K. Morokuma, O. Farkas, J. B. Foresman, and D. J. Fox, Gaussian, Inc. Wallingford CT, Wallingford CT, 2016.